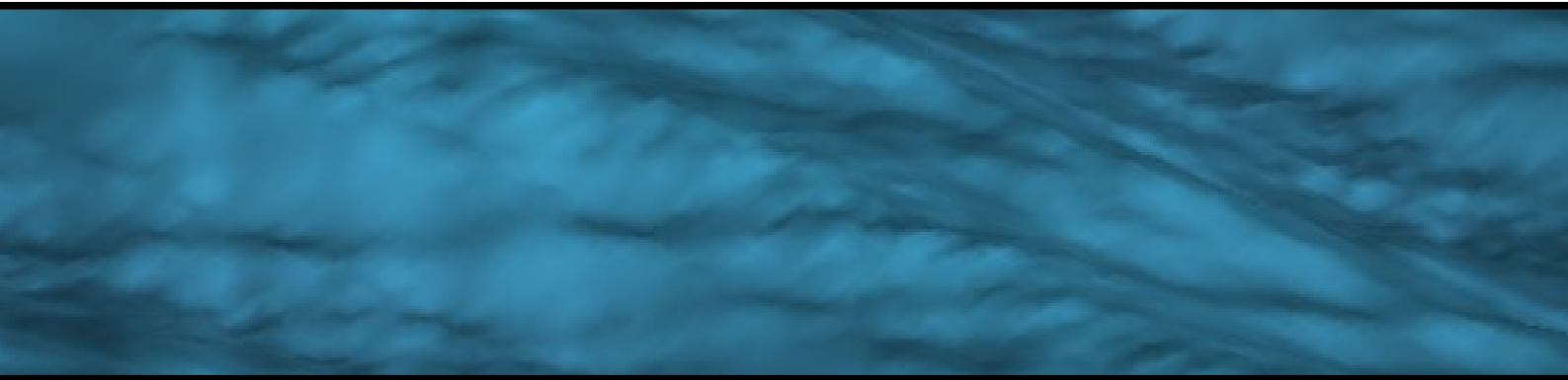


Determination of waves in three dimensions



Master's Thesis by Morten Jakobsen
Structural and Civil Engineering
Aalborg University 2011

Synopsis:

Title:
Determination of waves in three dimensions.

Theme:
Definitions and explanations of incident and reflected waves using various methods.

Project period:
Autumn 2010 - Spring 2011

Author:

Morten Møller Jakobsen

Supervisors:
Peter Bak Frigaard

Editions: 3

Number of pages in Main report: 48

Number of pages in Appendices: 26

Completed: 16-06-2011

Multi-directional waves are generated and analyzed theoretically based on the three dimensional wave spectra. The generation of waves covers both wave fields containing only incident waves and waves with both incident and reflected waves. These waves are then analyzed based on a piecewise constant method and later by the Maximum Likelihood Method. To verify the results commercial software is used and compared with the results obtained from the implemented methods. Additionally wave series obtained from IAHR are analyzed to determine the reliability of the implemented analyzing methods. The wave gauge array used in this project is the CERC 5 gauge array. To determine the resolution of the directional wave spectra obtained by the CERC array it is compared to alternative wave gauge arrays.

Preface

This project is written as a Master Thesis by Morten Jakobsen in 2011.

The project consists of two written parts, the main report and the appendices. It includes a DVD containing the data series, scripts and analysis results.

The focus of the main report is on the choices made and the results obtained throughout the report, while the appendices is explaining in a more in-depth and technical fashion the methods involved in the process. The main report is written with the intent to be read through and through, while the appendices are intended to be used for lookup.

Citations are made in the Harvard style by surname and publication year in the text, with the year in parentheses. If multiple publications has been made by the same author in the same year, uniqueness is obtained by a trailing alphabetic index. The literature list will be alphabetically sorted by surname and should contain enough information needed to obtain the original publication.

Summary

Studiet af bølger er omfangsrigt og derfor fokuserer dette projekt på et begrænset aspekt af dette område. Konkret vurderes egenskaberne for bølger i 3D gennem stokastisk analyse, herunder specifikt bestemmelse af spredningsfunktionen og retnings bølge spektret.

Igennem dette projekt bliver trykmålere anvendt, hvilke er placeret så bestemmelse af bølgehøjde og bølgeretning er mulig. Dette projekt har en teoretisk tilgang til emnet i den forstand, at computer implementeringer er lavet til både generering og analyse af bølger. Disse implementeringer er beskrevet sammen med en gennemgang af teorien der ligger til grund for metoderne. Det betyder også, at hverken felt eller laboratorieundersøgelser er udført.

De metoder der er implementeret er, for generering af bølger, irregulære bølger i både 2D og 3D. For 3D bølger er der både implementeret med og uden refleksion. Til at analysere disse bølger er hensigten derpå at implementere en stykvis konstant metode, en Maximum Likelihood Method og en modificeret version af Maximum Likelihood Method.

For at kontrollere at disse implementeringer giver fornuftige resultater, er de sammenlignet med en eksisterende software pakke, Wavelab og en værktøjskasse til Matlab kaldet DIWASP. Senere bruges implementeringerne til at analysere bølge serier med kendte egenskaber fra IAHR, The International Association for Hydro-Environment Engineering and Research, Hawkes (1997), der blandt andet indeholder bølger målt i et laboratorium.

Opsætningen af bølgemålerne er baseret på CERC opstillingen, hvor fem tryk målere er brugt. For at vurdere om dette valg er fornuftigt beskrives og implementeres en metode til bestemmelse af kvaliteten. For at kunne vurdere kvaliteten sammenlignes CERC arrayet med alternative opsætninger.

Table of Contents

| | | |
|----------|---|-----------|
| 1 | Introduction | 1 |
| 1.1 | Problem formulation | 1 |
| 2 | Introduction to multi-directional waves | 3 |
| 2.1 | The process | 3 |
| 3 | The implementations | 7 |
| 3.1 | Unidirectional waves | 7 |
| 3.2 | Generation of multi-directional, unimodal waves | 10 |
| 3.3 | Analysis of multi-directional waves | 13 |
| 3.4 | The piecewise constant method | 15 |
| 3.5 | The Maximum Likelihood Method | 17 |
| 3.6 | Generation of multi-directional, bimodal waves | 18 |
| 3.7 | The modified Maximum Likelihood Method | 19 |
| 4 | Implementation evaluation | 21 |
| 4.1 | Unidirectional waves | 21 |
| 4.2 | Unimodal waves | 24 |
| 4.3 | Bimodal waves | 30 |
| 4.4 | IAHR wave data | 37 |
| 5 | Optimization of wave gauge array | 41 |
| 6 | Conclusion | 47 |

List of Symbols

| | |
|----------------|--|
| a | Wave amplitude [m] |
| $D(f, \theta)$ | Spreading function |
| f | Frequency [Hz] |
| f_N | Nyquist frequency [Hz] |
| f_p | Peak frequency [Hz] |
| g | Gravitational acceleration [m/s^2] |
| h | Water depth [m] |
| H | Wave height [m] |
| H_s | Significant wave height [m] |
| H_{m0} | Zero-moment wave height [m] |
| k | Wave number [m^{-1}] |
| l_G | Gauge distance [m] |
| L | Wave length [m] |
| N | Sample size |
| r | Reflection coefficient |
| s | Spreading parameter |
| $S(f)$ | Frequency spectrum [Hz] |
| $S(f, \theta)$ | Directional wave spectrum [Hz] |
| t | Time [s] |
| T_s | Length of sample [s] |
| T_p | Peak period [s] |
| $C_{xy}(f)$ | Coincident spectral density function |
| $Q_{xy}(f)$ | Quadrature spectral density function |
| η | Wave elevation from MWL [m] |
| Γ | Gamma function |
| ω | Cyclic frequency [Hz] |
| $\Phi(f)$ | Spectral density matrix (one-sided power density function) |
| $\Phi_{xx}(f)$ | Auto-spectral density function (one-sided) |
| $\Phi_{xy}(f)$ | Cross-spectral density function (one-sided) |
| Ψ | Phase [m] |
| θ | Azimuth angle [rad/deg] |
| \Re | Real value |
| \Im | Imaginary value |

Introduction

The study of oceanic waves is a large field, and as such this project focuses on a limited aspect of it, the estimation of the properties of multi-directional waves through stochastic analysis.

Throughout this project only arrays of pressure gauges are used, which are used to obtain the water elevation. For simplicity these are referred to simply as wave gauges and wave gauge arrays. This project is mostly an theoretical approach to the subject in the sense that computer implementations of both the generation and analysis of the waves are used based on existing theoretical methods. This also means that neither field nor laboratory tests are performed.

In order to verify these implementations, they are first compared to existing software packages. Later the implementations are compared with actual wave records with known properties from IAHR, The International Association for Hydro-Environment Engineering and Research, Hawkes (1997). Further tests are performed with these models to examine the setup of the wave gauge arrays in an attempt to test existing wave gauge setups against each other and if possible improve the array layout.

1.1 Problem formulation

The aim of this project is to determination of three dimensional wave spectra, getting familiar with the use of existing methods. Examining the methods assumptions and limitations. Creating scripts to determine the spreading function of wave series numerically. Working with the IAHR laboratory wave series, to test the implemented methods against the uncertainties introduced by waves created in the laboratory. Experimentation will be made in regards to the placement of the wave gauges trying to improve on existing gauge array designs.

In short:

- Obtain knowledge of 3D wave properties.
- Obtain knowledge of the methods used to determine the spreading function and the directional spectrum.
- Create a new method to determine the spreading function.
- Determine uncertainties involved with numerical and experimental tests.

Introduction to multi-directional waves

Oceanic waves may be interpreted in varying levels of detail, where a compromise between simplicity of the model and the computational time required for more complex models must be made. In this chapter the basic theory will be outlined, with attention to the basics of the analytical aspect of generation and analysis of irregular waves.

A more in-depth explanation of generation and analysis is presented in chapter 3. The chapter will cover both a more in-depth explanation as well as an explanation of the implementations in this project. The idea is to present an analyzing method and explain the strengths and weaknesses, supported by tests with different types of computer- and laboratory generated waves.

The two main reasons why this project covers generation of waves is first and foremost to get familiar with the concepts of wave spectra in both two(x and z) and three dimensions(x,y,z). Furthermore the methods used to generate the waves can be controlled and modified as more advanced analysis are presented.

2.1 The process

Natural occurring waves are influenced by a wide range of sources, among the more noteworthy of those are the effects of the slope of the seabed, wind and lunar gravitation. Due to the complexity of the influences, observing natural occurring waves reveals wave properties such as the wave heights and wave-periods to appear random. It is in other words necessary to simplify the interpretation of waves.

The commonly used simplification is to assume that waves can be interpreted as a stochastic process, which means that the mean and correlation functions may be obtained to represent statistical properties of the natural occurring waves at any time. From this assumption a stochastic analysis may be performed, which consists of calculation in the time, frequency and probabilistic domain.

By doing so a commonly accepted interpretation of the the ocean waves are used, where a directional spectrum is to be estimated, which represents the characteristics of the waves. The directional spectrum consists of a (one-dimensional) frequency spectrum and a directional spreading function (referred to simply as the spreading function in this project), see figure 2.1.

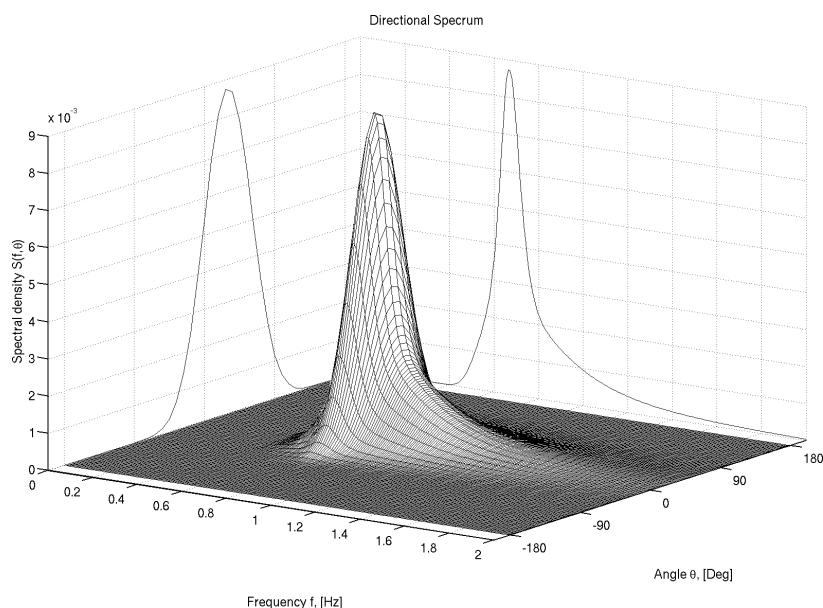


Figure 2.1: Visual interpretation of the directional wave spectrum, where the contour lines represent the spreading function and the frequency spectrum.

The one-dimensional frequency spectrum defines the characteristics of the waves while the spreading function determines the angular distribution of these one-dimensional wave characteristics.

The first step in the stochastic analysis requires sample functions which are obtained in the time domain through measurements of the oceanic waves. This can be done in several ways, the method used in this project is through wave gauges measuring the elevation. Then the auto- and cross-correlation functions are calculated from the sample functions. Using the obtained correlation functions, the spectral density functions are estimated, which are a part of the frequency domain.

In order to determine the directional properties, probabilistic methods are used, among the most common are: The Maximum Likelihood Method, MLM, the Maximum Entropy Method, MEM, and the Bayesian Direct Method, BDM.

While this project only implements the MLM, the BDM method are introduced indirectly through commercial software packages. It is beyond the point of this project to determine the strengths and weaknesses of each method. Instead the focus is on determining the accuracy of the implementation through crosschecking with the available methods in the commercial software, assuming that the results shared by most methods are the most likely solution.

The commercial software packages used to generate and analyze the sample functions are:

- DIWASP, by MetOcean Solutions LTD (2002), A Matlab toolbox, which can be used to calculate using, either of the four methods.
- Wavelab, by Andersen (2010), A standalone program, which can be used to calculate using both the MLM and BDM method.

To further test the implementations, several wave series with known properties are used, which are provided by IAHR, The International Association for Hydro-Environment Engi-

neering and Research, Hawkes (1997).

Other factors than the method used to analyze the sample functions affect the results. In a simulation environment the number of uncertainties lowers dramatically but the layout of the wave gauge array still has a significant role on the results. In order to obtain good results the placement of these gauges should be considered carefully. Throughout the initial testing the CERC 5 gauge array introduced by Borgman and Panicker (1970) is used. This setup provides reasonably good results with only five wave elevation gauges, see figure 2.2.

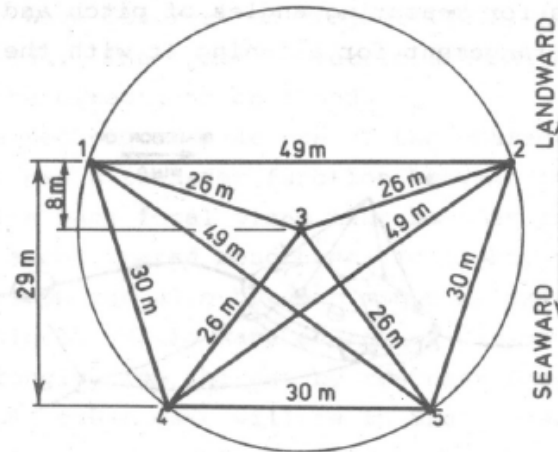


Figure 2.2: CERC 5 gauge setup here with minimal gauge distance of 26 m.

When the implementation and testing of the generation and analyzing methods are done the intent is to examine alternative placements and change the amount of gauges to find a good compromise between the precision they provide and the complexity of the array.

The implementations

This chapter covers both an explanation of the theory of the methods as well as an explanation of the implementations made in this project. The idea is to present both methods used to generate sample functions and methods which can analyze and estimate the properties of these sample functions. The methods implemented may vary from the procedures suggested by the source material, in these cases an explanation of the choices made within these methods is presented.

The ordering of the methods presented here is arranged after the time of implementation. This means that first the generation method is introduced and then the corresponding analysis is explained.

In this report multi-directional are divided into two categories, uni-modal and bi-modal waves. The term uni-modal and bi-modal refer to the spreading function which can contain either just the incident waves (uni-modal) or a combination of both incident and reflected waves (bi-modal).

Notice that black and white models are conceptual models while colored models are results from the implementations.

The list of methods implemented are:

1. Irregular wave trains send strictly along the main-axis, these waves are referred to as unidirectional waves.
2. Multi-directional waves containing only incident wave trains, the waves generated are called unimodal due to shape of the spreading function.
3. Multi-directional waves containing both incident and reflected wave trains, referred to as bimodal waves.

3.1 Unidirectional waves

By assuming that the sample functions may be considered as stochastic processes it is implied that the records must be ergodic random waves. Further simplifications are made by excluding calculation of effects of the seabed (shoaling, refraction, and diffraction) and by considering only first order waves. The assumptions made in the implemented method is that waves may be considered as an infinite amount of super-positioned regular waves, based on Pierson et al. (1955).

The basic formula used to create regular waves is shown in equation (3.1).

$$\eta(x, t) = a \cdot \cos(k \cdot x + \omega \cdot t + \Psi) \quad (3.1)$$

Where $\eta(x, t)$ is the wave elevation which depends on position x and time t . The right hand side consists of the a cosine expression with amplitude a , the circular frequency ω , the time t , the wave numbers k , the position x and the phase Ψ .

By superposition of all frequencies in equation (3.1) the expression for irregular waves are shown in equation (3.2).

$$\eta(x, t) = \sum_{\omega} a_{\omega} \cdot \cos(k_{\omega} \cdot x + \omega \cdot t + \Psi_{\omega}) \quad (3.2)$$

To recreate realistic waves a spectrum is introduced which is based on the Hasselmann et al. (1973) modeling of the Jonswap field experiments, which where performed in the North Sea in the period from 1968 to 1969. To avoid having to determine the governing fetch parameter the implementation in this project will be based on the rewriting done by Goda (1988), which is based on the significant wave height and peak period, referred to as the Jonswap spectrum. Using the implemented method and the parameters shown in table 3.1 it is expected that the generated model should create a Jonswap spectrum as shown in figure 3.1.

| T_p | H_s | h | T_s | N | x |
|-------|-------|-------|--------|-----|-------------|
| 1.5 s | 0.2 m | 0.6 m | 50 min | 512 | [0, 1, 2] m |

Table 3.1: Values of the parameters used in the example.

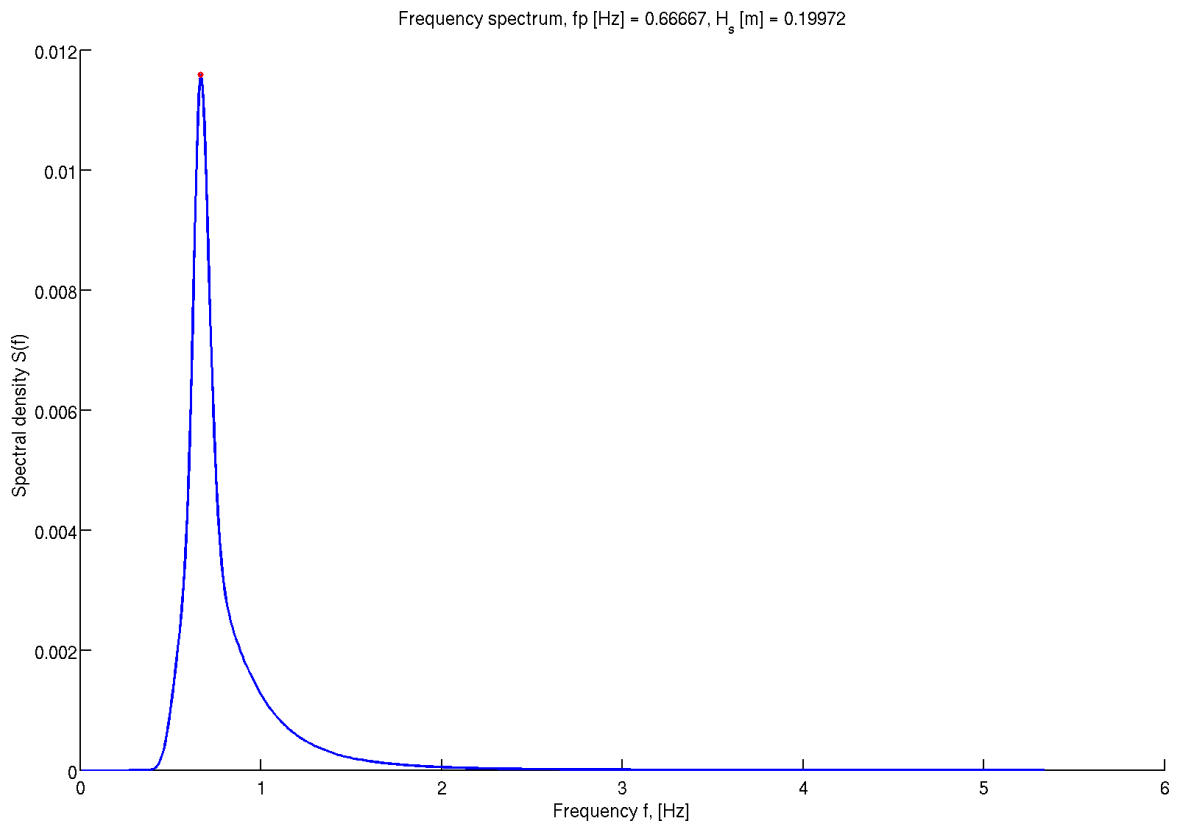


Figure 3.1: Expected Jonswap spectrum based on the parameters specified in the example.

Through analysis it should then be possible to obtain a similar Jonswap spectrum. In order to obtain this spectrum the procedure described by Bendat and Piersol (2000) is used, where the ensemble-averaged auto-spectral density estimates are computed. In this section only the procedure is explained, see appendix A.2 for a more detailed explanation. The essence of this procedure is listed below:

1. Compute the mean value of the data record and subtract this value from the record.
2. Divide the data record into n_d continuous blocks containing N elements each. In this implementation 50% overlap is used.
3. To suppress side-lobe leakage, taper the data values of each block x_n by the Hanning window. While some literature suggests limiting the taper size to only cover a certain percentage of the ends of each block, the window is applied to the entire block in this implementation.
4. Compute the Fast Fourier Transform for each block.
5. Adjust scale factor $X(f_k)$ for loss from tapering.
6. Compute the auto-spectral density estimate, $\Phi_{xx}(f)$.

In this case several wave gauges are used, and to utilize these extra auto-spectra the frequency spectrum estimate $\hat{S}(f)$ is obtained by an average of the available auto-spectra as seen in

equation (3.3).

$$\hat{S}(f) = E[\Phi_{xx}(f)] \quad (3.3)$$

Where E is the average of auto-spectra available. The resulting frequency spectrum is shown in figure 3.2.

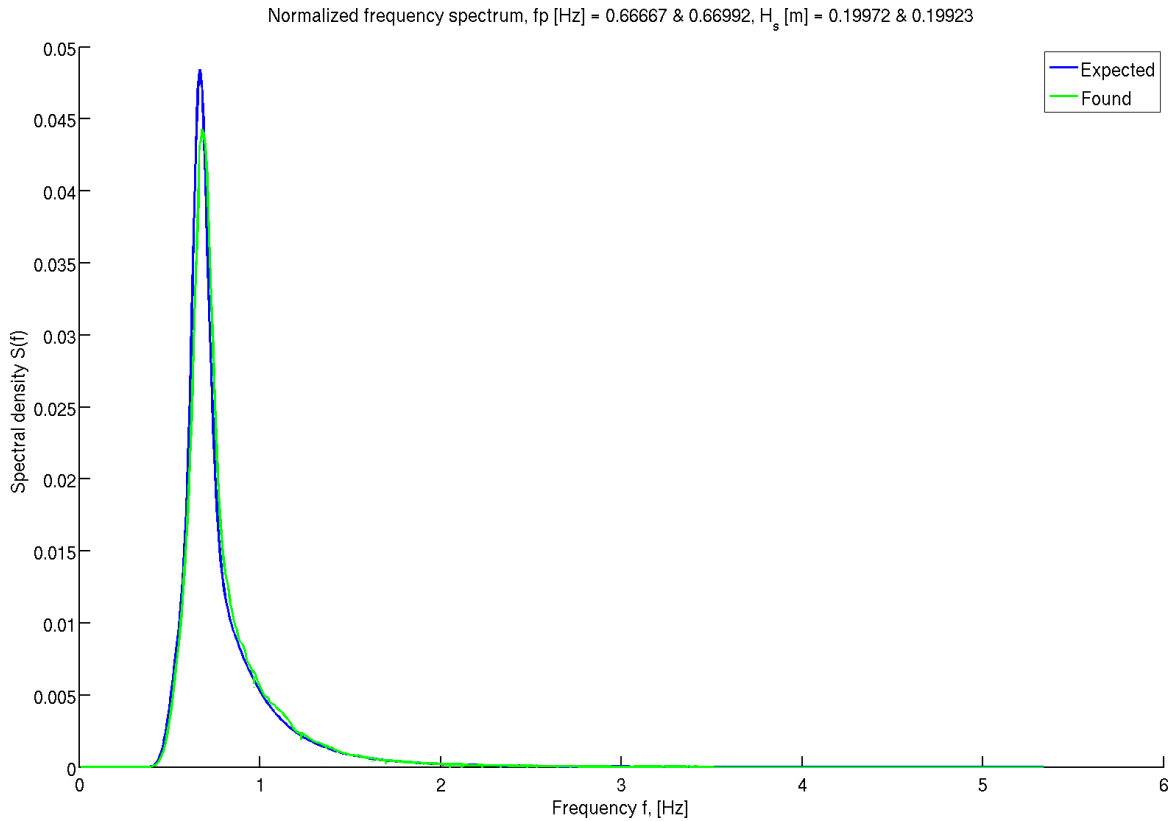


Figure 3.2: Comparison of the expected Jonswap spectrum and the frequency spectrum obtained through analysis.

3.2 Generation of multi-directional, unimodal waves

For multi-directional waves the solution has been to extend the unidirectional solution to the (x, y) -plane defining the wave propagation direction as components of x and y . This is illustrated in equation (3.4).

$$\eta(x, y, t) = \sum_{\omega} \sum_{\theta} a_{\omega\theta} \cdot \cos(k_{\omega} \cdot x \cdot \cos(\theta) + k_{\omega} \cdot y \cdot \sin(\theta) + \omega \cdot t + \Psi_{\omega\theta}) \quad (3.4)$$

Where θ is the wave propagation direction and Ψ is now a function of both frequency and direction. In order to progress from regular to irregular waves equation (3.4) is superpositioned of both frequency and direction. The initial phase is chosen at random within a cosine period $\Psi \in]0; 2\pi]$.

In order to cover multi-directional waves it is necessary to incorporate a spreading function,

$D(f, \theta)$, to determine how the waves spread from the main direction. The spreading function is principally based on both frequency and azimuth range, but in this implementation it is constant for all frequencies.

Combining the Jonswap spectrum and the spreading function results in the directional wave spectrum, $S(f, \theta)$, see equation (3.5).

$$S(f, \theta) = S(f) \cdot D(f, \theta) \quad (3.5)$$

The directional wave spectrum may also be visually interpreted seen in figure 3.3.

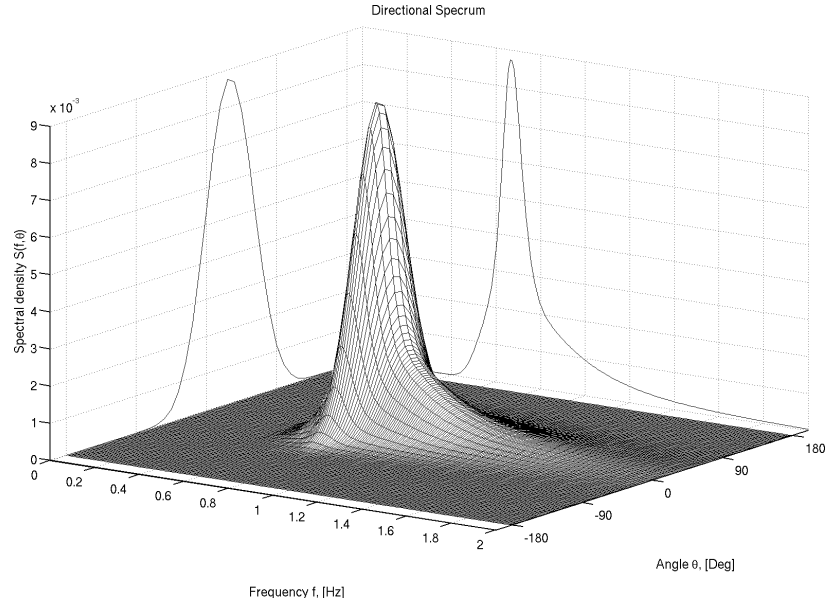


Figure 3.3: Interpretation of the directional wave spectrum.

The spreading function creates an angular distribution of the energy of the one-dimensional spectrum this means that the spreading function must be normalized as seen in equation (3.6).

$$\int_{-\pi}^{\pi} D(f, \theta) d\theta = 1 \quad (3.6)$$

The distribution function used in this project is based on Mitsuyasu et al. (1975) named the Mitsuyasu spreading function hence forth. An more in-depth explanation is covered in appendix B. The expression is shown in equation (3.7).

$$D(f, \theta) = \frac{2^{2s-1} \Gamma^2(s+1)}{\pi \Gamma(2s+1)} \cos^{2s} \left(\frac{\theta - \theta_0}{2} \right) \quad (3.7)$$

The spread parameter, s , varies with frequency and wave type, where the wave types may be fetch or wind generated or a combination of the two according to Mitsuyasu et al. (1975). In the implementations the spreading function is set to a constant value for all directions. With the directional wave spectrum equation (3.5), and the basic wave equation equation (3.4) the waves may be generated.

To test the methods strength against noise in the acquired samples a random noise function,

rnl , is used, which is defined as a percentage of the significant wave height, as seen in equation (3.8).

$$rnl(x, y, t) = rnd(x, y, t) \cdot \frac{nl \cdot (1 + (1 - r))}{2} \quad (3.8)$$

where nl is the factor of the noise level, r is the reflection coefficient, which is zero in the absence of reflection and rnd is random values between 0 and 1, with the size equal to the wave series $\eta(x, y, t)$. Finally the new wave elevation can be calculated using equation (3.9).

$$\eta = \eta_0 + \eta_0 \cdot rnl \quad (3.9)$$

Using the implemented method and the parameters shown in table 3.2 it is expected that the generated model should create a directional spectrum as shown in figure 3.4. Where the minimum distance of the gauge pairs are 0.2 m.

| T_p | H_s | h | T_s | N | n_θ | θ_0 | s | Array type |
|-------|-------|-------|--------|------|------------|------------|-----|------------|
| 1.5 s | 0.2 m | 0.6 m | 50 min | 1024 | 41 | 0 deg. | 12 | CERC5 |

Table 3.2: Values of the parameters used in the example.

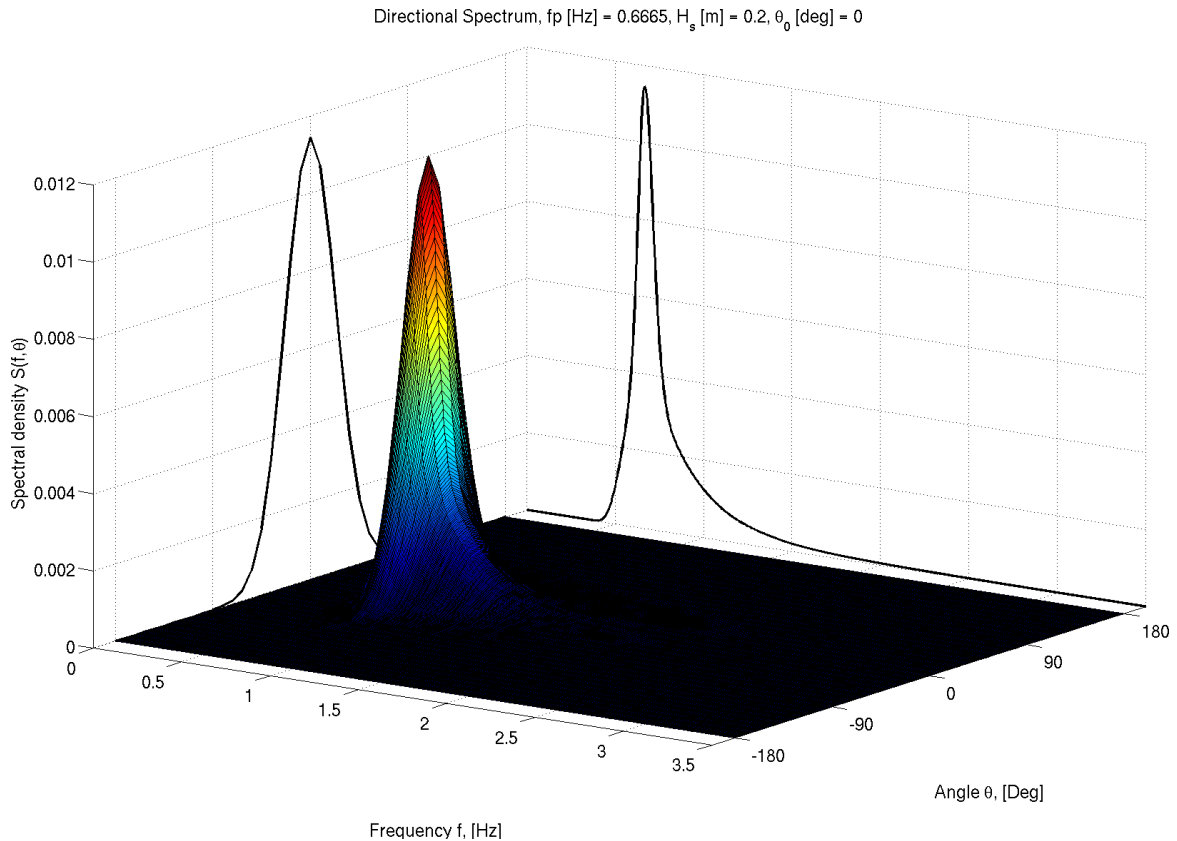


Figure 3.4: Expected directional spectrum based on the parameters specified in the example.

3.3 Analysis of multi-directional waves

The central concept of the wave analysis used in this project is the assumption that waves may be characterized by the directional spectrum defined in equation (3.5). With this in mind the aim is to obtain the spreading function $D(f, \theta)$ and the frequency spectrum $S(f)$, as this will result in having the directional spectrum too.

The frequency spectrum is calculated by the same procedure as the unidirectional waves. So the remaining unknown, the spreading function, is then found by the following derivation. The exponential form of the elevation is used as seen in equation (3.10).

$$\eta(x, y, t) = a \cdot \Re \left(e^{i(\omega t + k(x \cos(\theta) + y \sin(\theta)) + \Psi)} \right) \quad (3.10)$$

Where \Re is the symbol used for real values. The conversion is obtained by Euler's formula shown in Appendix E.3.1. The amplitude a may be defined in terms of the directional spectra seen in equation (3.11).

$$a = \sqrt{2S(f, \theta)\Delta f \Delta \theta} \quad (3.11)$$

Where Δf and $\Delta \theta$ represents a small section of the discretized directional spectra and a is the volume under the red rectangle, illustrated in figure 3.5

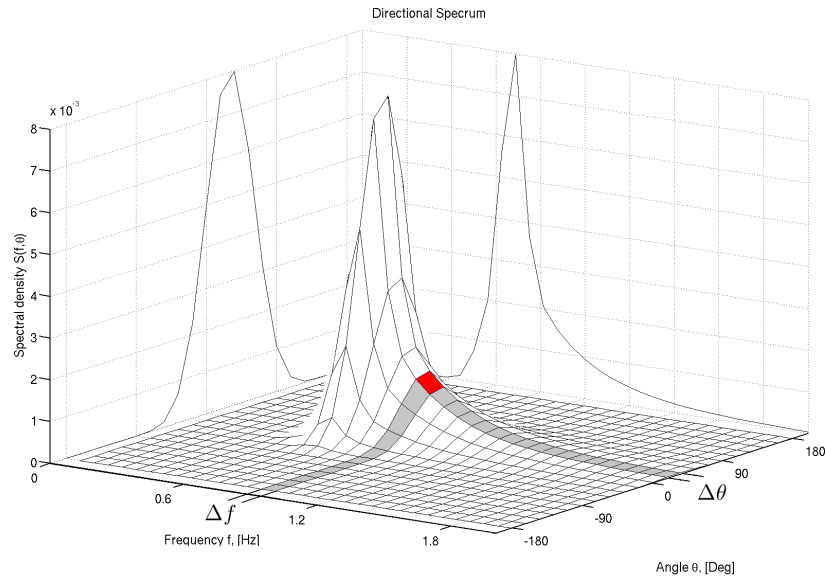


Figure 3.5: Discretized directional spectra.

The cross-correlation of the elevation between two sample functions η_x and η_y is defined as equation (3.12). Using equation (3.10), equation (3.10), equation (3.11) and the Wiener-Khinchine theorem shown in appendix E.3.2, equation (3.13) is obtained.

$$R_{xy}(\tau) = \frac{1}{T} \int_0^T \eta_x(t) \eta_y(t + \tau) dt \quad (3.12)$$

$$\Phi_{xy}(f) = \int_{-\pi}^{\pi} S(f, \theta) e^{ikr \cdot \cos(\theta - \beta)} d\theta \quad (3.13)$$

where β and r represent the angle and distance between the two wave gauges. Using equation (3.5), (3.3) and (3.13) the expression can be reformed into equation (3.14), which is the central equation for multi-directional waves.

$$\frac{\Phi_{xy}(f)}{\Phi_{xx}(f)} = \int_{-\pi}^{\pi} D(f, \theta) e^{ikr \cdot \cos(\theta - \beta)} d\theta \quad (3.14)$$

Using equation (3.14) the spreading function $D(f, \theta)$ can be estimated. But in order to determine the spreading functions some assumptions must be made.

The commonly used method is to model the spreading function by a function such as the Fourier series or the cosine squared function mentioned in section 3.1, which can both be defined by an arbitrary amount of variables. By adjusting the function so it contains more equations than unknown the system becomes overdetermined and probabilistic methods are then used to obtain an estimate.

The entire analysis procedure is illustrated in figure 3.6, including determination of the spreading function by using probabilistic methods such as the Maximum Likelihood Method, the Maximum Entropy Method and the Bayesian Deterministic Method.

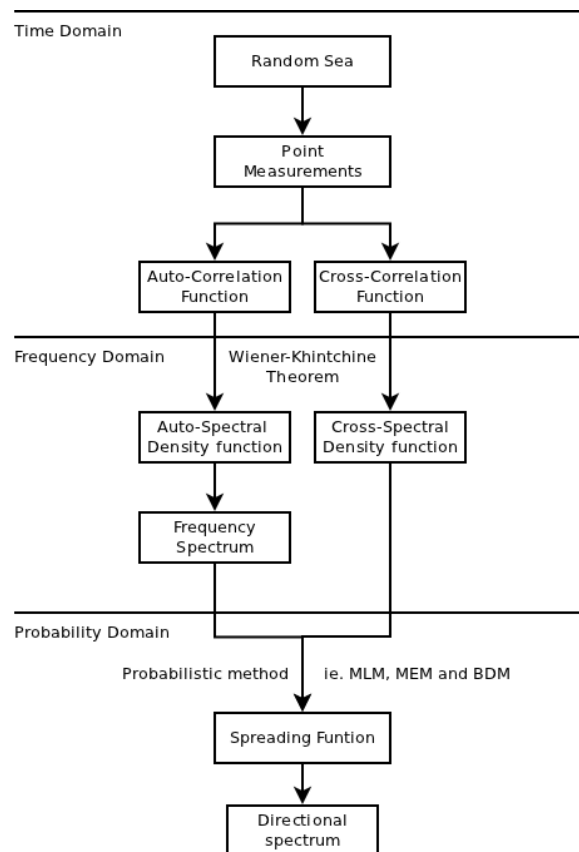


Figure 3.6: Stochastic analysis process.

3.4 The piecewise constant method

A method named the piecewise constant method is implemented based on equation (3.14), where one equation is created for each gauge pair available. This allows a solution which can be solved without using probabilistic fitting methods. Hence equation (3.14) may be interpreted as the equation (3.15).

$$\frac{\Phi_{xy}(f)}{\Phi_{xx}(f)} = \sum_{n=1}^N \mathbf{D}(f, \theta_n) e^{i\mathbf{k}\mathbf{r} \cdot \cos(\theta_n - \beta)} \cdot \Delta\theta_n \quad (3.15)$$

Where θ_n is a discretization of θ into N angular ranges. From this simplification the directional spectrum will end up discretized in N directions.

In this implementation the cross- and auto-spectra are obtained through equation (3.16) with the complete spectral estimation procedure described in appendix A.

$$\begin{aligned} \Phi_{xy}(f) &= C_{xy} - iQ_{xy} \\ \text{where :} \\ C_{xy} &= \frac{2}{T} (\Re(X)\Re(Y) + \Im(X)\Im(Y)) \\ Q_{xy} &= \frac{2}{T} (\Re(X)\Im(Y) - \Im(X)\Re(Y)) \end{aligned} \quad (3.16)$$

C_{xy} and Q_{xy} are the coincident- and quadrature-spectra of the Fourier transforms $X(f, T)$ and $Y(f, T)$, and \Re and \Im are the real and imaginary parts of the Fourier transforms. The distances r and β are easily obtained through conversion of the Cartesian coordinates (the distance from gauge to gauge in both directions) to polar coordinates. Finally the wave numbers are calculated based on the dispersion relation, equation (3.17), using an convergence algorithm explained in appendix E.3.3.

$$\omega^2 = g \cdot \mathbf{k} \cdot \tanh(\mathbf{k} \cdot \mathbf{h}) \quad (3.17)$$

Analyzing the generated model in section 3.1 should then result in a directional spectrum similar to the spectrum in figure 3.7, with a wide spread but with the peak around 0.

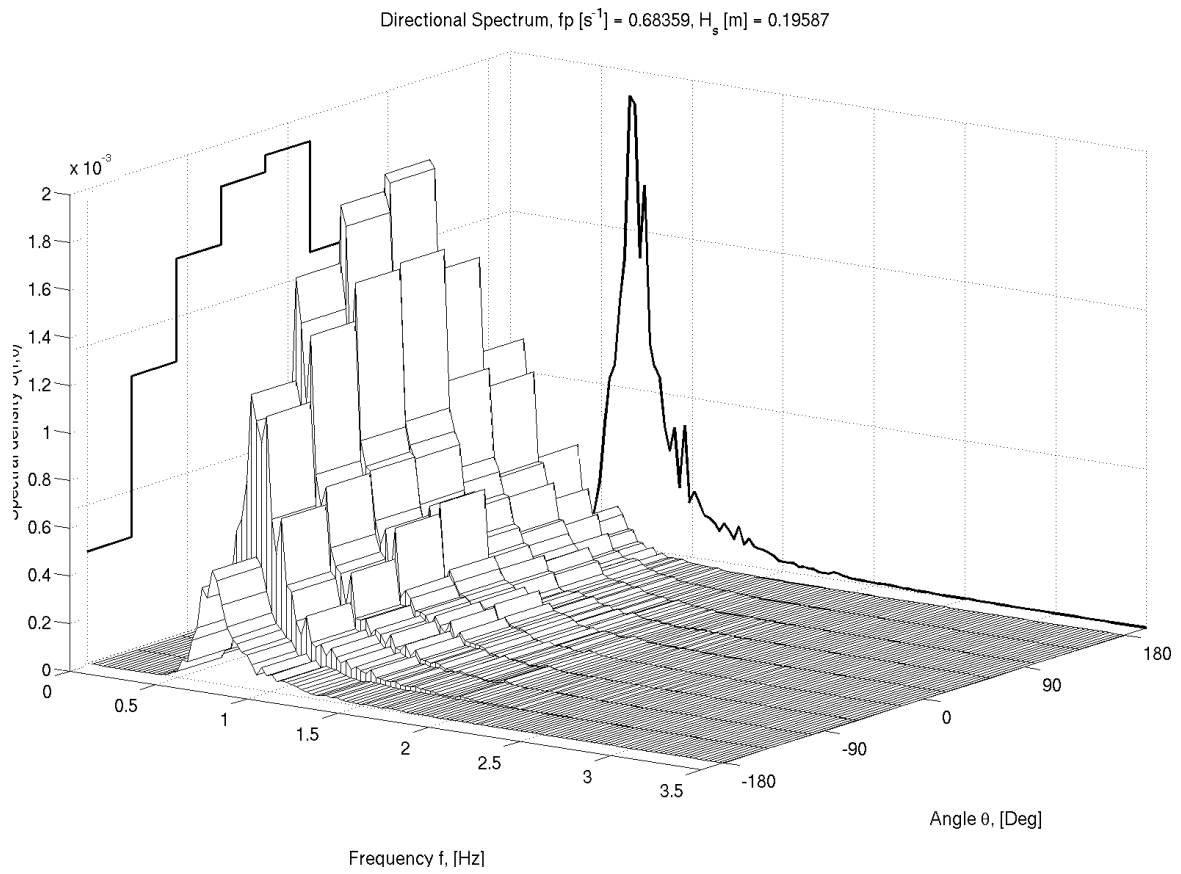


Figure 3.7: Expected directional spectrum for simple analysis.

However, using the generated data from section 3.1 the implemented method results in figure 3.8.

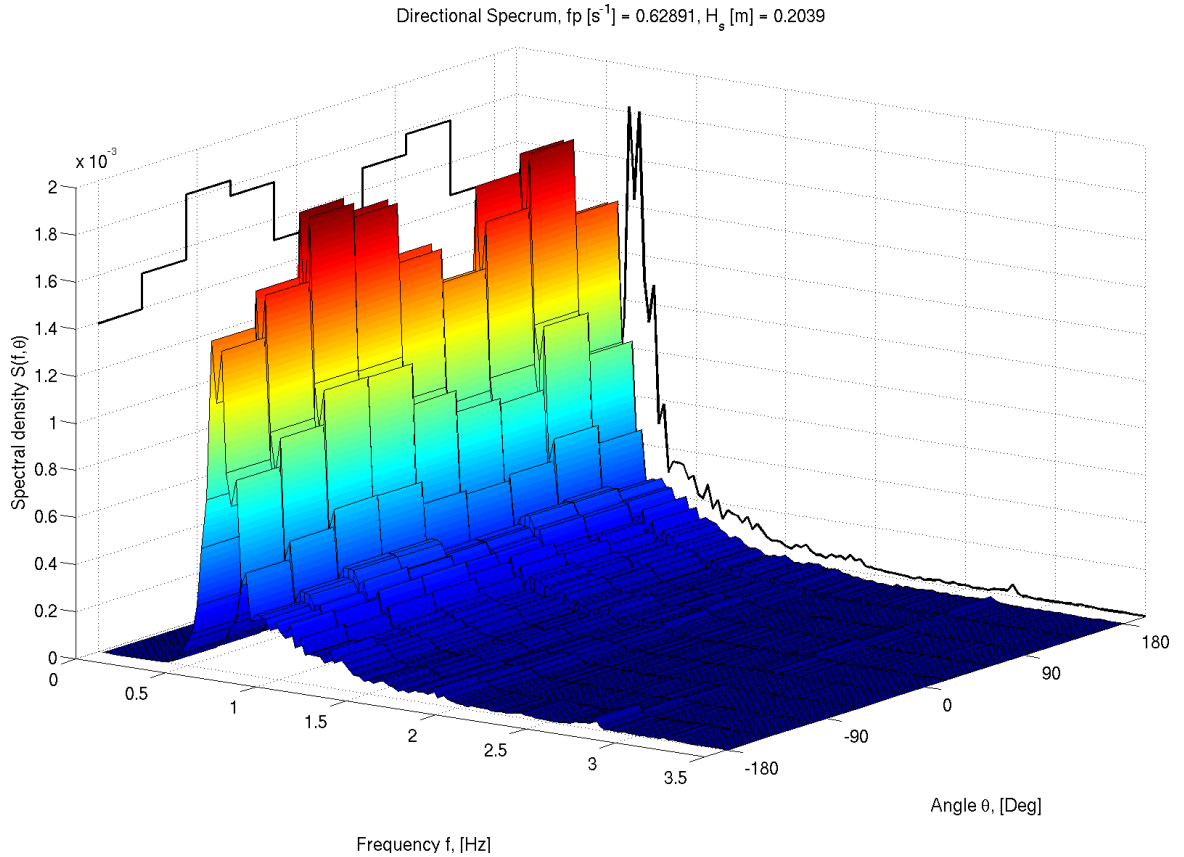


Figure 3.8: Directional spectrum for simple analysis.

The result obtained from the implementation are unsatisfying. Although extensive work has been performed to find the cause of the failure in the implementation no solution has been found. For this reason the implementation of this method is discontinued in this project.

3.5 The Maximum Likelihood Method

As an alternative to section 3.4 the Maximum Likelihood Method, MLM, is implemented. The method is primarily based on Davis and Regier (1977) supported by Isobe and Kondo (1984). A more throughout explanation of the MLM implementation is found in appendix C. The central expression of this method is the calculation of the spreading function seen in equation (3.18).

$$\hat{\mathbf{D}}_0(\mathbf{k}, \theta) = \kappa / \left[\sum_{m,n}^M \Phi_{mn}^{-1}(\theta) e^{i\mathbf{k}(\mathbf{x}_n - \mathbf{x}_m)} \right] \quad (3.18)$$

where κ is a variable which ensures that the expression satisfies the properties of the spreading function equation (3.6). M is the amount of wave gauges in the array and Φ_{mn}^{-1} is the inverse full spectral matrix. The spectral matrix is defined by $\Phi(x, y)$ and contains both cross- and auto-spectra, where the auto-spectra are found in the diagonal and the cross-spectra are the remaining off-diagonal entries, the properties of spectral matrix is further

explained and illustrated in appendix E.1.

The implementation in this project differs a bit from the procedure explained in the source literature, as the spectral matrix and the wave numbers in equation (3.18) are determined using the same approach as that of the discrete method. Another change is in determining κ , as mentioned in section 3.1 the spreading function is normalized and so κ is defined simply by dividing with the mean from the result of equation (3.18), see equation (3.19).

Then the directional spectrum is obtained by multiplying by the frequency spectrum, equation (3.20). Note that the frequency spectrum is obtained by average of the auto spectra, just as in the discrete method.

$$\hat{\mathbf{D}} = \frac{\hat{\mathbf{D}}_0}{E[\hat{\mathbf{D}}_0]} \quad (3.19)$$

$$\hat{\mathbf{S}}(f, \theta) = \hat{\mathbf{S}}(f) \cdot \hat{\mathbf{D}}(f, \theta) \quad (3.20)$$

Using the generated file from section 3.1 the MLM method obtains an estimate, seen in figure 3.9.

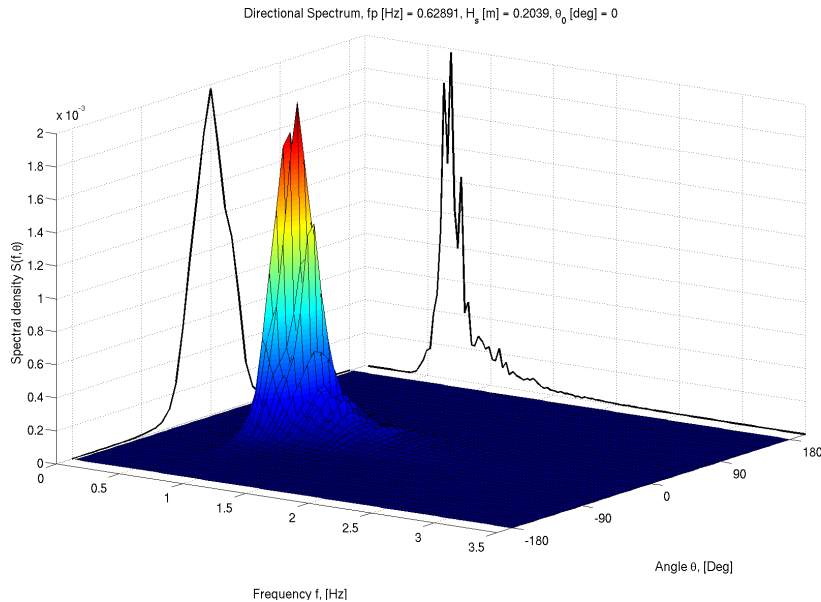


Figure 3.9: Generation model.

This result is far more satisfying, and this method is subject to more throughout testing which is done in chapter 4.

3.6 Generation of multi-directional, bimodal waves

Until now only uni-modal waves have been considered which are sufficient if there are no more than one main direction of the waves. But due to disturbances in the water influenced by shorelines and structures it is often relevant to incorporate reflecting waves into the expression. To calculate reflected waves it is necessary to include an additional function into the spreading function resulting in a bi-modal spreading function.

But as explained in appendix E.2, reflection is quite complex, as the reflection coefficient and distance to the reflector may vary with the frequency and slope of the reflector.

The method used to generate bi-modal waves is based on two peak directions (θ_{0i} and θ_{0r}), then two time series are generated with a constant phase shift difference, still retaining a random phase for each frequency.

Two input methods are created, one where the two peak directions are specified manually and one which only takes an incident peak direction, and then calculate the second peak direction using provided information on the direction and distance to the reflection line.

3.7 The modified Maximum Likelihood Method

In this section the more advanced Modified Maximum Likelihood Method, MMLM, is examined. The method is based on Isobe and Kondo (1984). This modified method is introduced as the standard MLM is inaccurate in distinguishing between incident and reflected waves in a bimodal spectrum. One of the problems with the traditional MLM is that it is assumed that a random phase lag between the incident and reflected waves are used. As explained in greater detail in appendix E.2 this assumption is incorrect. With a reflector in the vicinity there exists a direct relation between the phase of the incident and reflected waves however. This is what the MMLM is created to account for by adding a phase-interaction term.

Just as in the discrete method, the spectral matrix is calculated using the procedure described in appendix A. The spreading function of the MMLM is shown in equation (3.21).

$$\hat{D}(\mathbf{k}, \sigma) = \kappa / \begin{cases} \sum_{m,n}^M \Phi_{mn}^{-1}(\sigma) e^{i\mathbf{k}(\mathbf{x}_n - \mathbf{x}_m)} & r_0 \leq 0 \\ \sum_{m,n}^M \Phi_{mn}^{-1}(\sigma) e^{i\mathbf{k}(\mathbf{x}_n - \mathbf{x}_m)} - \frac{\left\{ \sum_{m,n}^M \Phi_{mn}^{-1}(\sigma) [e^{i\mathbf{k}(\mathbf{x}_n - \mathbf{x}_{mr})} + e^{i\mathbf{k}(\mathbf{x}_{nr} - \mathbf{x}_m)}] \right\}^2}{4 \sum_{m,n}^M \Phi_{mn}^{-1}(\sigma) e^{i\mathbf{k}(\mathbf{x}_{nr} - \mathbf{x}_{mr})}} & r_0 > 0 \end{cases} \quad (3.21)$$

Where $\hat{D}(\mathbf{k}, \sigma)$ is a estimate of the spreading function and κ is a proportionality constant determined in the same way as in the MLM. r_0 is the initial estimated reflection coefficient and x_{nr} and x_{mr} are the positions of x_n and x_m mirrored in the reflection line. The spreading function is very similar to the MLM, in fact it is the same expression that is used when no reflections are present. The difference is the term which are being subtracted when reflections exist. In order to calculate r_0 the Isobe and Kondo (1984) proposed the expression in equation (3.22).

$$r_0 = - \frac{\sum_{m,n}^M \Phi_{mn}^{-1}(\sigma) [e^{i\mathbf{k}(\mathbf{x}_n - \mathbf{x}_{mr})} + e^{i\mathbf{k}(\mathbf{x}_{nr} - \mathbf{x}_m)}]}{2 \sum_{m,n}^M \Phi_{mn}^{-1}(\sigma) e^{i\mathbf{k}(\mathbf{x}_{nr} - \mathbf{x}_{mr})}} \quad (3.22)$$

It should be noted that equation (3.22) can contain negative values which is not possible for a reflection coefficient. This is of no importance to equation (3.21) though, as it is regarded

in the same way as a reflection coefficient of zero and does not influence the calculations in this range. To obtain a better reflection coefficient estimate \hat{r} all negative values are set to zero as shown in equation (3.23).

$$\hat{r} = \begin{cases} 0 & r_0 \leq 0 \\ r_0 & r_0 > 0 \end{cases}$$

In order to determine the coordinates x_{nr} and x_{mr} of the mirror image of the array some knowledge must be determined and/or assumed. Two conditions are considered in this project, the first is where the direction of the reflection line is known and only the distance is calculated, the second is where neither direction nor distance to the reflection line is known. Davidson et al. (1998) has suggested a method to determine the estimate of the distance to the reflection line based on a linear least squares regression between the numerator and denominator of equation (3.23).

$$\kappa(\sigma) = \frac{\Phi_{mm}(\sigma)}{\int_{\mathbf{k}_i} \left[\hat{S}(\mathbf{k}_i, \sigma) + 2\sqrt{\hat{S}(\mathbf{k}_i, \sigma)\hat{S}(\mathbf{k}_r, \sigma)} \cos \cdot \mathbf{k}_i(x_m - x_{mr}) + \hat{S}(\mathbf{k}_r, \sigma) \right] d\mathbf{k}_i} \quad (3.23)$$

This final step of the MMLM implementation could unfortunately not be finished in time for the project dead-line. The MMLM is implemented to the point where it can be used in the case where the distance and direction of the reflection line is known.

Implementation evaluation

The next step is to examine the accuracy of the implemented methods. This is done by extensive testing of both generating and analyzing implementations. The complete list of simulations are found on the DVD in the *Datafiles* folder, in this section only the highlights will be presented.

The waves evaluated are separated into sections covering the generated waves with unidirectional, multi-directional waves and the wave series from the IAHR project, Hawkes (1997).

All tests generated by the implementations in this project has no noise applied and while some tests (included on the DVD) has been performed to test the noise functionality in the scripts it should be noted that the possibility to add noise has not been as thoroughly tested as intended.

In this section references are made to execution times of the implementations, this is based on a 2 GHz dual core computer with 2 GB ram.

4.1 Unidirectional waves

For the unidirectional simulations the comparisons made in this project relies on the differences between the model which is expected from the generating method and the model found in the analysis. The wave properties that are compared are the significant wave height, peak frequency and the overall match of the frequency spectrum. The significant wave height is obtained by equation (4.1) and (4.2). The generating method is using the properties shown in table 4.1, while the analyzing method strictly uses information on h and x from the generated series, with $N = 256$.

| T_p | H_s | h | T_s | N | x |
|-------|-------|-------|--------|-----------|-------------|
| 1.5 s | 0.2 m | 0.6 m | 50 min | 64 – 1024 | [0, 1, 2] m |

Table 4.1: Values of the parameters used in the unidirectional case.

$$H_s \simeq 4 \cdot \sqrt{\sum_{xx} \Phi_{xx} \cdot \Delta f} \quad (4.1)$$

$$dif_{H_s} = \left| 1 - \frac{H_{s,generated}}{H_{s,expected}} \right| \cdot 100\% \quad (4.2)$$

The difference in peak frequency is essentially obtained in the same way as the significant wave height equation (4.2). The peaks are found by obtaining the maximum value of the frequency spectrum. The overall difference in the frequency spectrum is found by equation (4.3).

$$dif_f \sum_f \frac{|f_{generated} - f_{expected}|}{2} \cdot 100\% \quad (4.3)$$

The only parameter which affects the results significantly is the resolution of the frequency spectrum shown in figure 4.1.

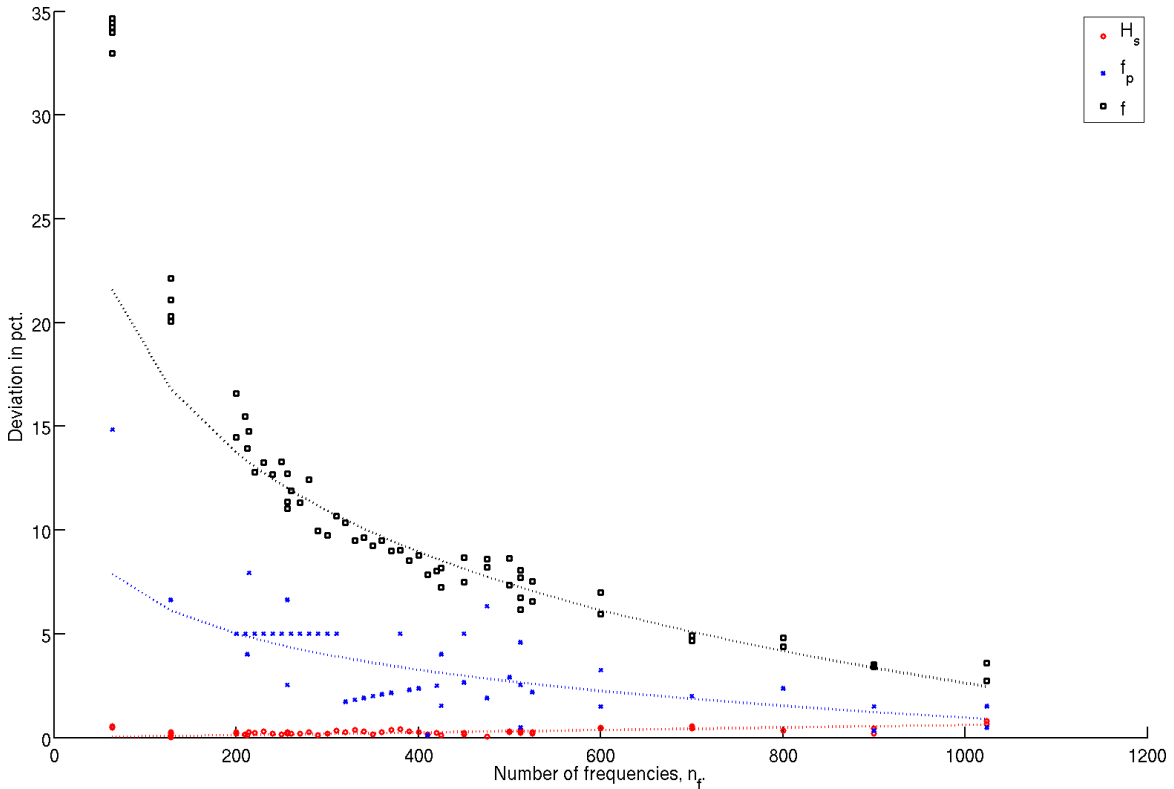


Figure 4.1: Deviation in percent of f_p , H_s and the frequency spectra f as the frequency resolution is varied.

This relates to an improvement from a frequency resolution of $N = 64$ with 33 pct. deviation seen in figure 4.2 to $N = 1024$ with 4 pct. in figure 4.3.

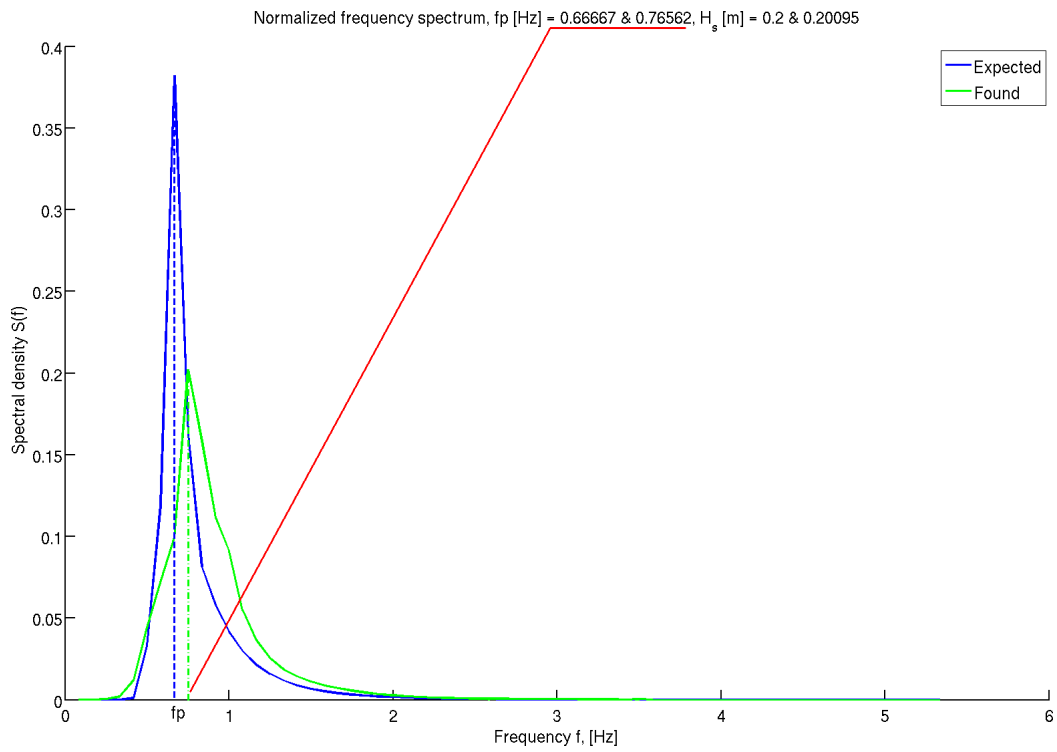


Figure 4.2: Frequency spectrum with a frequency resolution of 64.

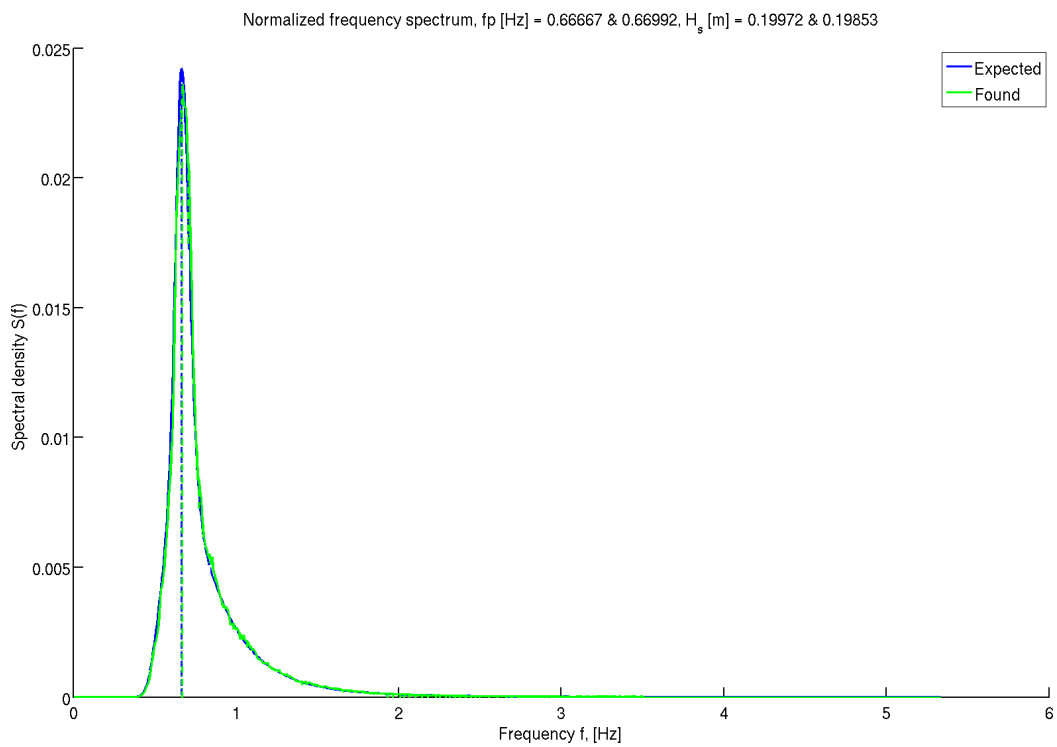


Figure 4.3: Frequency spectrum with a frequency resolution of 1024.

4.2 Unimodal waves

The second test is of the unimodal generating model and the corresponding MLM implementation. As the discrete method never provided any reasonable results it is omitted from this section. For the bidirectional cases the spreading function is compared using the same principle as the comparison of the frequency spectrum. Starting by modifying the frequency resolution as in the unidirectional case and the properties shown in table 4.2, it is seen in figure 4.4 that the deviation first improves significantly with $N \geq 2048$.

| T_p | H_s | h | T_s | N | n_θ | θ_0 | s | Array type |
|-------|-------|-------|--------|------------|------------|------------|-----|--------------|
| 1.5 s | 0.2 m | 0.6 m | 50 min | 64 – 16384 | 41 | 0 deg. | 12 | <i>CERC5</i> |

Table 4.2: Values of the parameters used in the unimodal case.

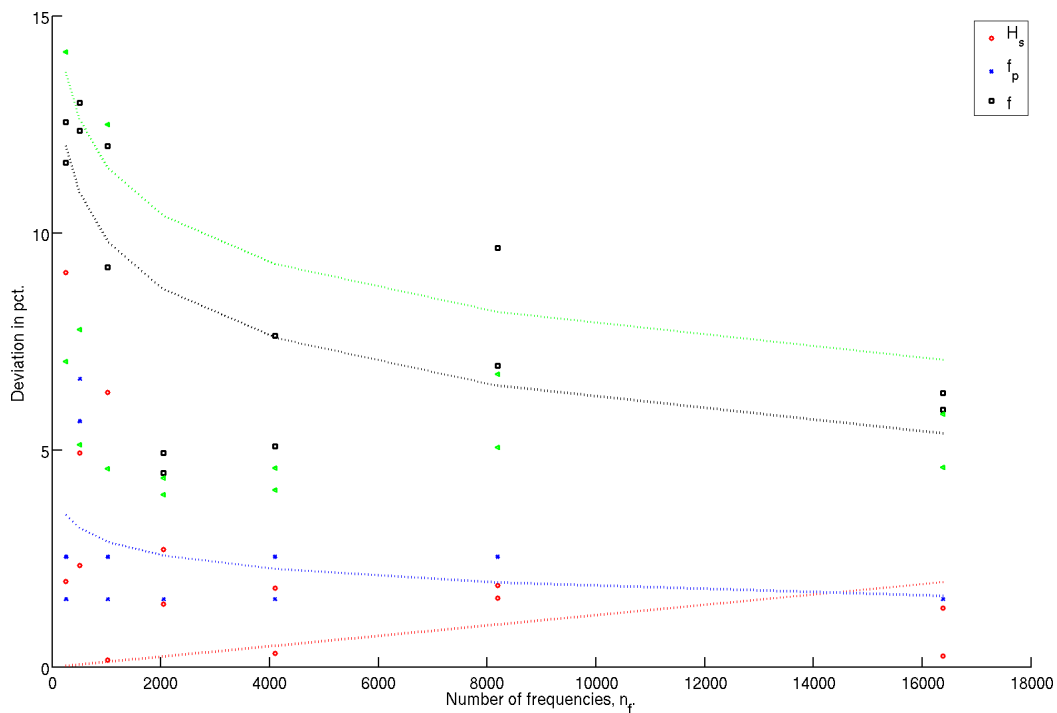


Figure 4.4: Comparison of f_p , H_s , the unimodal frequency spectrum and spreading function.

This is illustrated by the expected generated model in figure 4.5, the model found in the MLM implementation in figure 4.6, the comparison between the two frequency spectra in figure 4.7, the comparison of the spreading functions in figure 4.8 and the results of the BDM analysis in Wavelab figure 4.9.

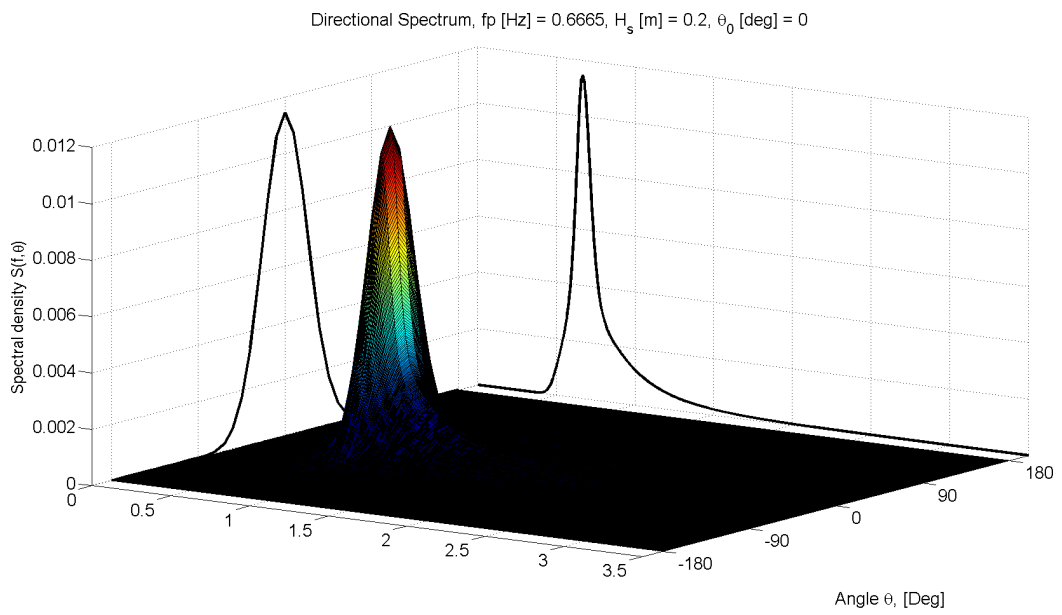


Figure 4.5: Expected generated directional spectrum with a frequency resolution of 2048.

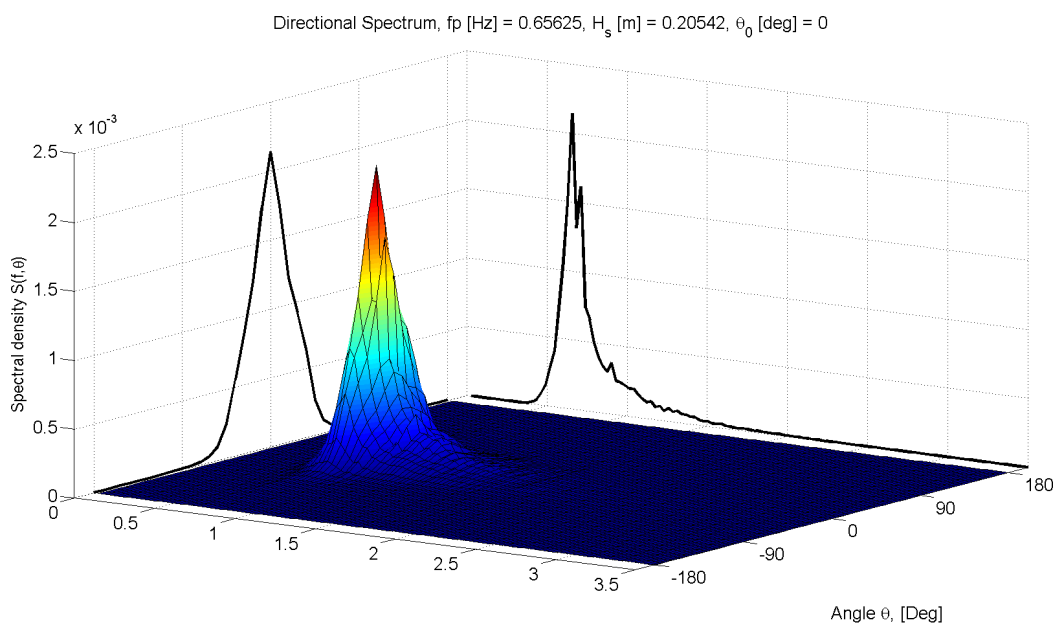


Figure 4.6: Directional spectrum obtained from the MLM.

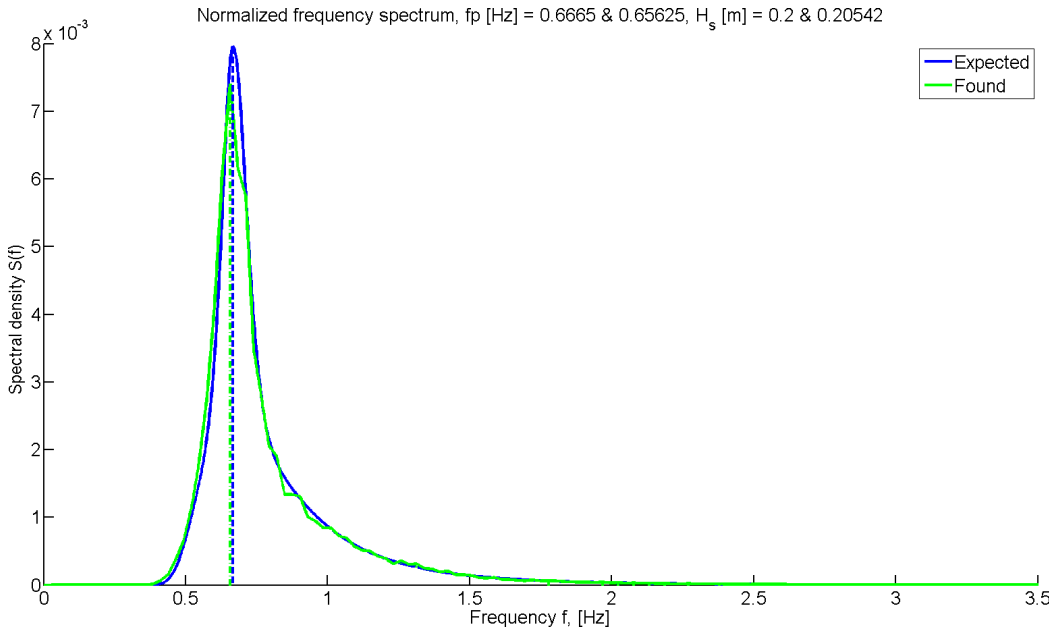


Figure 4.7: Comparison of the frequency spectra.

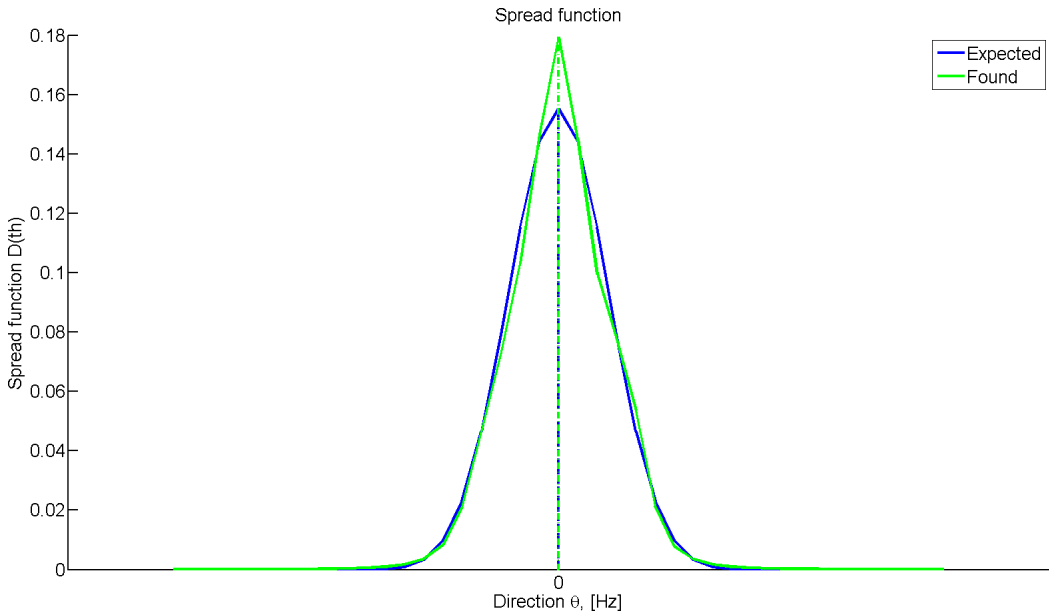


Figure 4.8: Comparison of the spreading functions.

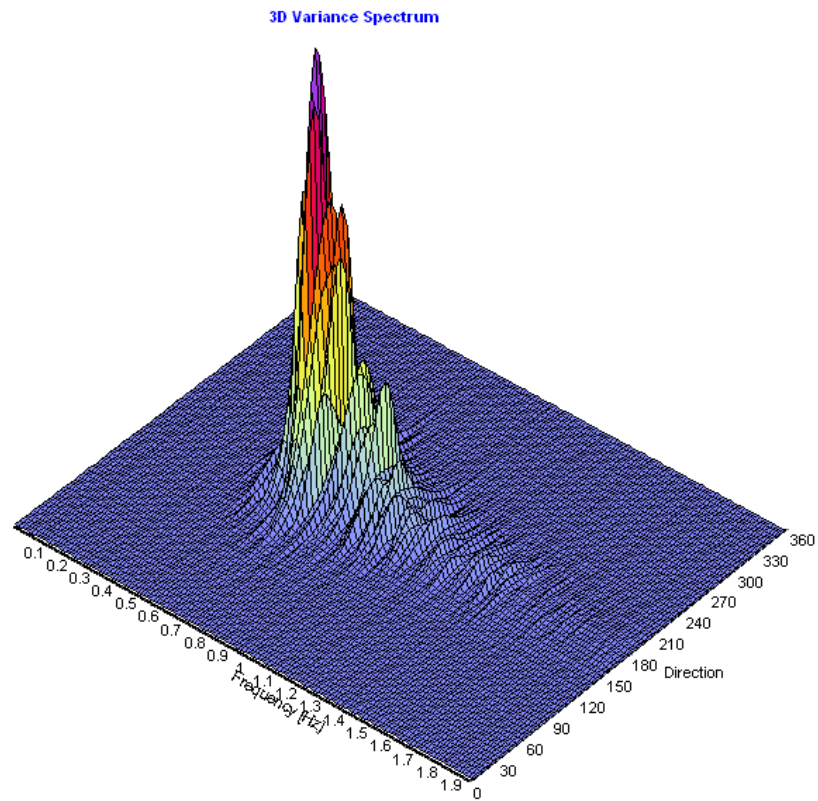


Figure 4.9: Analysis done in WAVELAB compared to the generated directional spectrum.

To compare the results of $N = 2048$, (2^{11}) above, the results of $N = 164384$, (2^{14}) is shown in figure 4.10, 4.11, 4.12, 4.13 and 4.14.

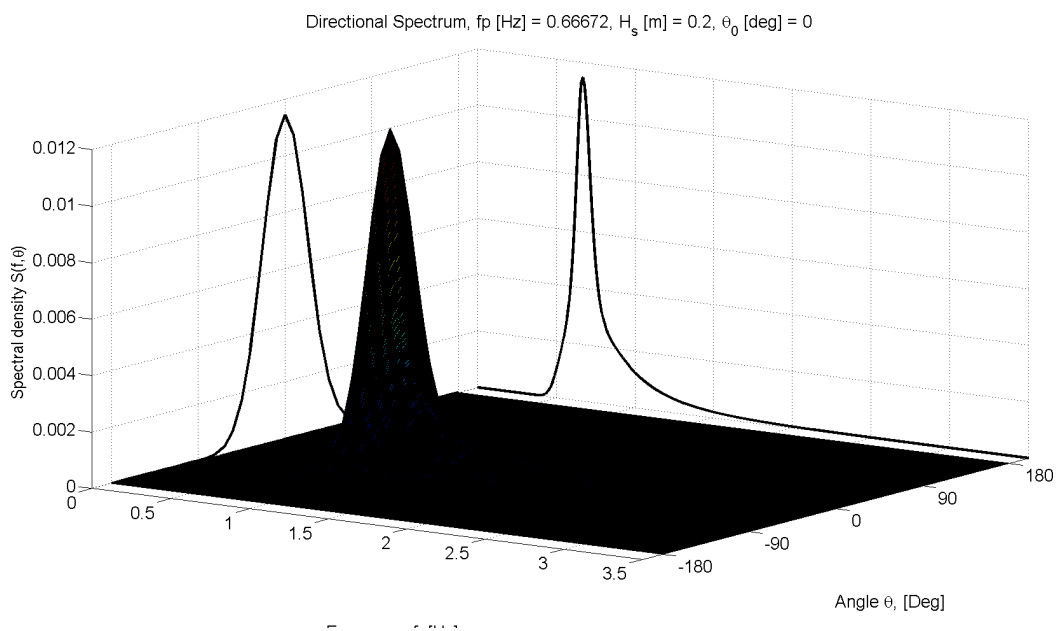


Figure 4.10: Expected generated directional spectrum with a frequency resolution $N = 2^{14}$.

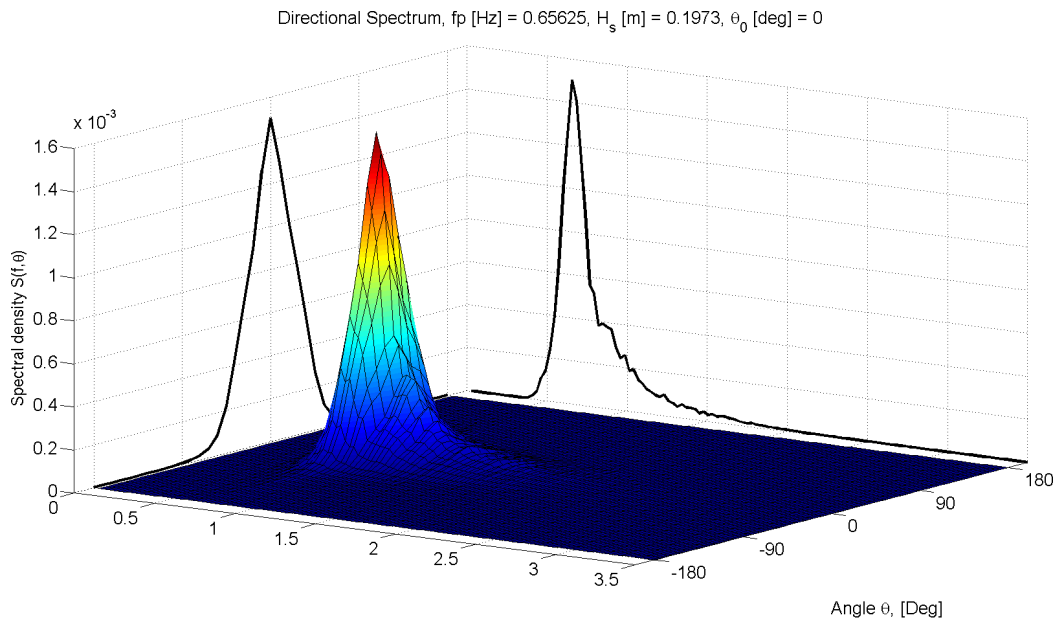


Figure 4.11: Directional spectrum obtained from the MLM.

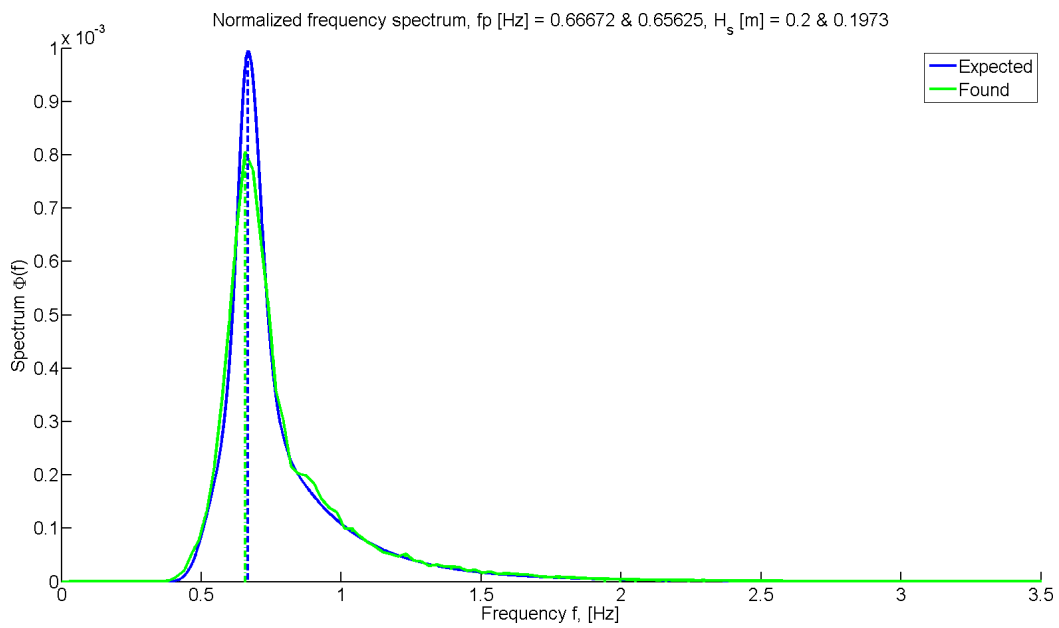


Figure 4.12: Comparison of the frequency spectra.

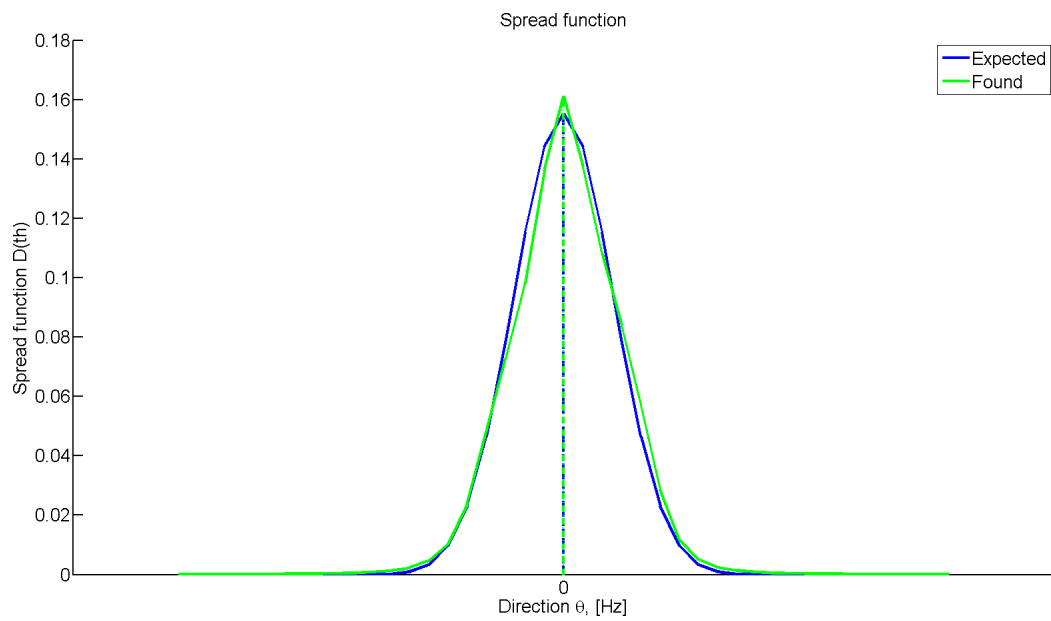


Figure 4.13: Comparison of the spreading functions.

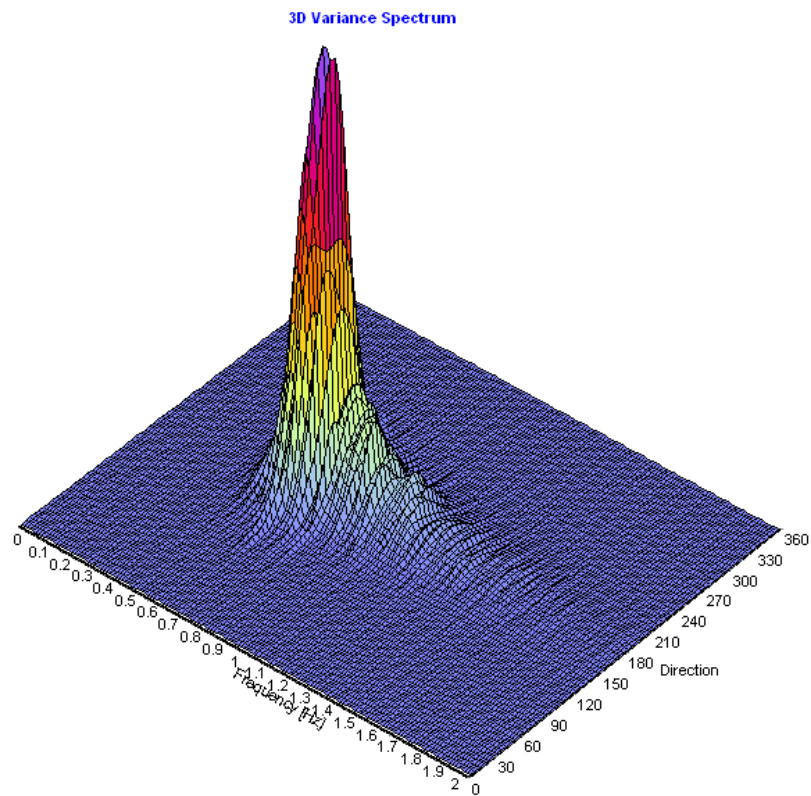


Figure 4.14: Analysis done in WAVELAB compared to the generated directional spectrum.

As seen there are no definitive improvement by increasing the frequencies alone. Another thing to notice in general is the relatively poor generation of the spreading function with

$n_{th} = 41$. In the context of testing the MLM implementation this is of minor importance, but to ensure the generating method works as intended this number is increased from 41 in steps of 10 to 101. The results are found on the DVD. This produces a smoother spreading function but does not produce better results between the expected generated model and the model found by the analysis.

For all the unimodal cases tested there are no notice worthy difference found between the results obtained from the MLM implementation and the BDM method used in Wavelab. The MLM should produce broader directional peaks according to Benoit and Teisson (1994). This could not be established in the unimodal tests performed in this report however.

On a final note the implemented method for generating bidirectional waves are running at $O(N^3)$ as no improvements are made in the transition from 2D to 3D. This results in unsatisfying long generating times where a simple test of $N = 2048$, $t = 50$ min and $s = 41$ requires around 25 minutes. This calculation time can be improved by using the random phase method utilizing the inverse Fourier transform. The random phase method is down prioritized though as the main focus in this project is the methods for analyzing waves.

4.3 Bimodal waves

The final test of the bimodal waves are performed and analyzed by the MLM implementation. The properties are the same as those found in table 4.2, only the number of frequencies used in the model is increased to 4096 along with three additional parameters, two of which relates to the reflection line and the reflection coefficient, these are specified in table 4.3.

| θ_r | l_r | r |
|------------|-------|-----|
| -30 deg | -1 m | 0.5 |

Table 4.3: Reflection line direction, θ_r , distance, l_r and reflection coefficient in the bimodal case.

This results in the gauge array seen in figure 4.15 and the corresponding directional spectrum obtained from the implemented MLM in figure 4.17.

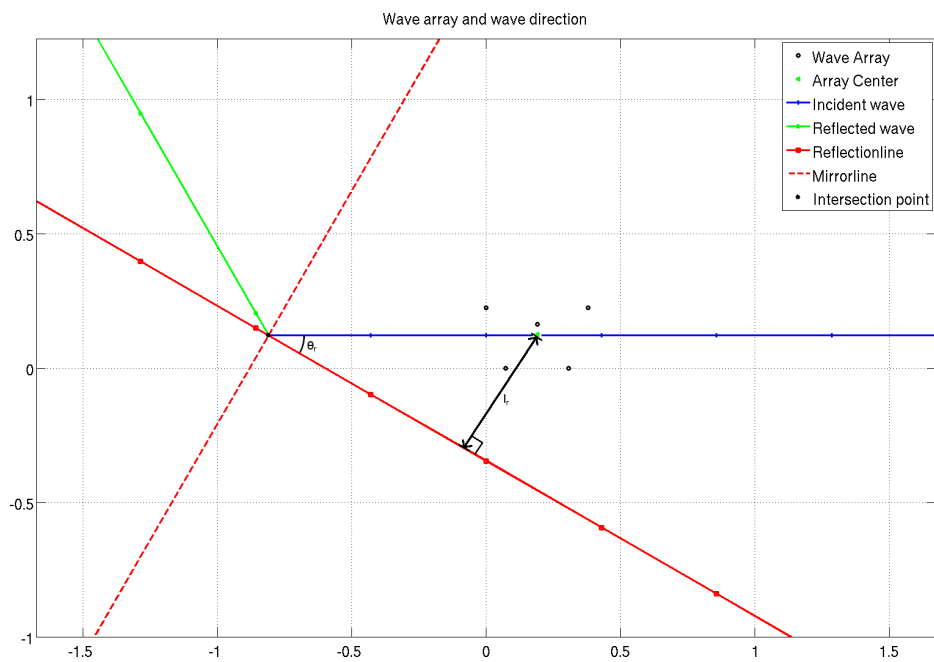


Figure 4.15: Wave gauge array with the incident and reflected wave direction along with the reflector.

This leads to the expected generated model seen figure 4.16.

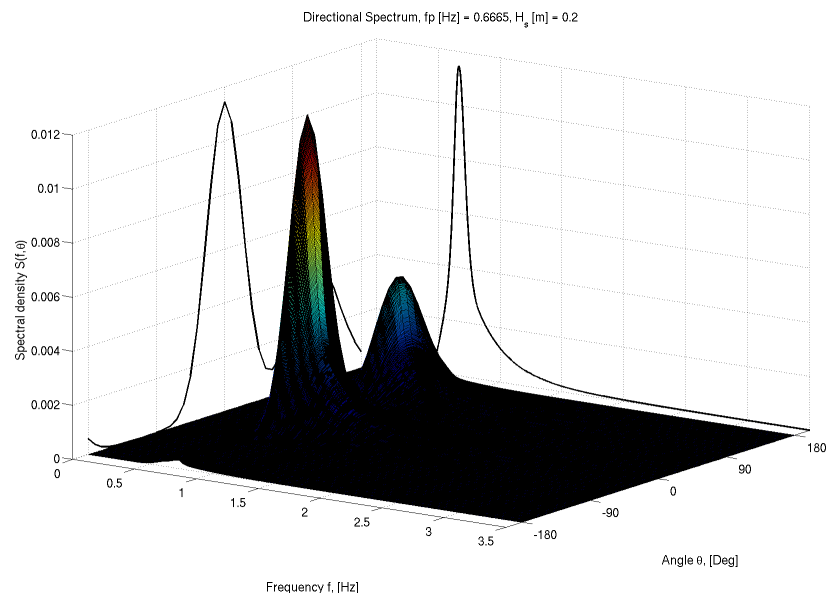


Figure 4.16: Expected generated directional spectrum with a frequency resolution $N = 4096$.

The results are seen in figure 4.17 and figure 4.18.

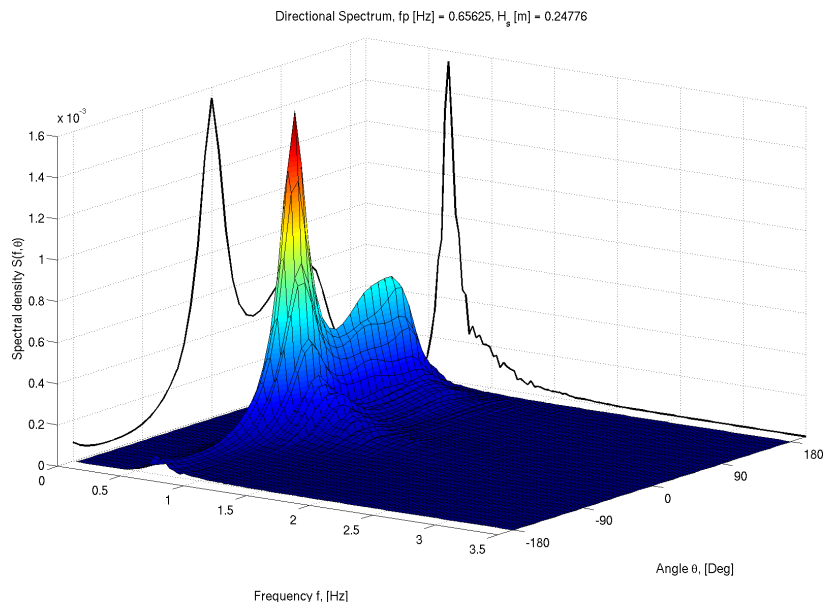


Figure 4.17: Directional spectrum obtained from the MLM.

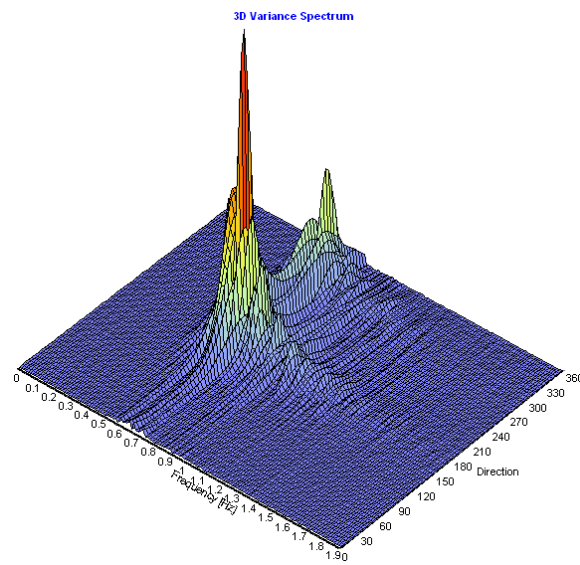


Figure 4.18: Directional spectrum obtained from Wavelab's BDM.

In figure 4.19 the comparison of the spreading functions of the implemented method are shown.

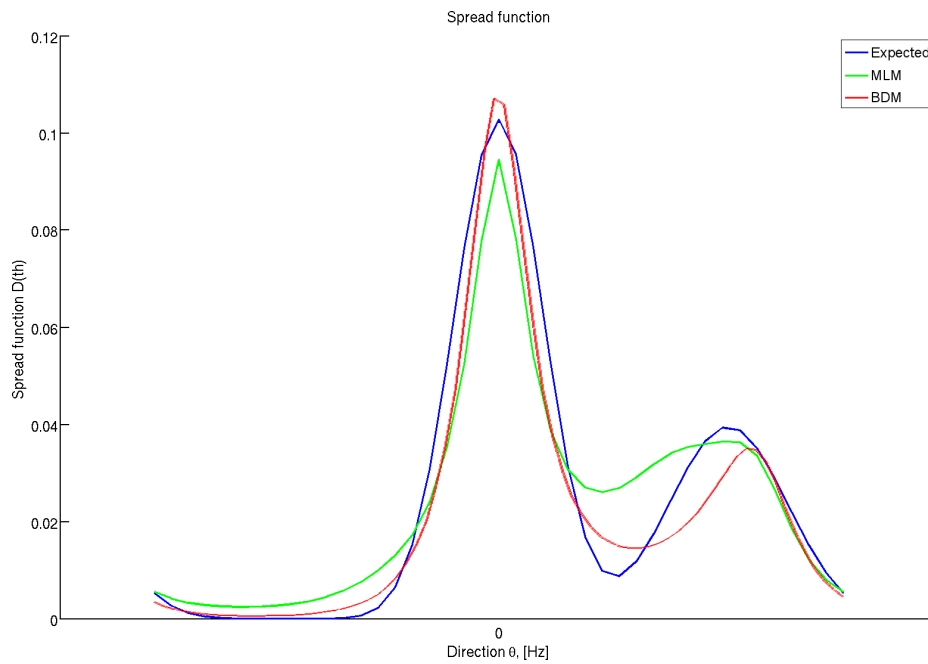


Figure 4.19: Comparison of the spreading functions.

While the peaks are located quite accurately by the implemented method the difference in the spreading functions are between 15 and 20 pct. Wavelab provides a better result at distinguishing between the incident and reflected waves, which are more similar to the expected model.

The generation of bimodal wave takes $O(2N^3)$ as two peak directions are calculated separately, this results in 50 min generation time, compared to the phase difference method in Wavelab which only takes roughly 2 min. For this reason only a limited amount of tests has been performed using the generating feature in the implemented method. Although the bimodal wave generation appears to work it has been producing unstable reflection coefficients according to Wavelab. To further test the implemented MLM three generated wave series are made in Wavelab. The parameters are shown in table 4.4.

| <i>Test</i> | H_s | h | θ_{i0} | θ_{r0} | r | s_i | s_r |
|-------------|-------|------|---------------|---------------|-----|-------|-------|
| 1 | 0.2m | 0.6m | 60 deg. | 100 deg. | 0.5 | 10 | 10 |
| 2 | 0.2m | 0.6m | 90 deg. | 180 deg. | 0.5 | 10 | 10 |
| 2 | 0.2m | 0.6m | 90 deg. | 270 deg. | 0.5 | 10 | 10 |

Table 4.4: Peak direction incident θ_{i0} , reflection θ_{r0} , spread parameter incident s_i , reflection s_r .

The spreading functions obtained from the Wavelab BDM analysis are shown in table 4.5 and figure 4.20.

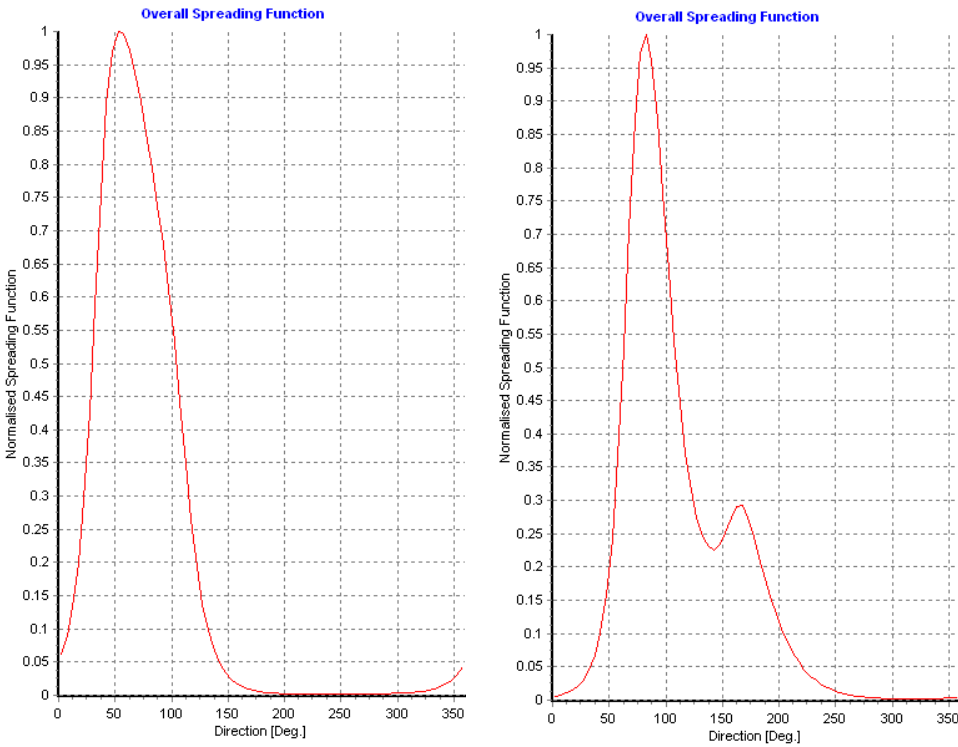


Table 4.5: Spreading function obtained from Wavelab's, on the left based on test 1 and 2.

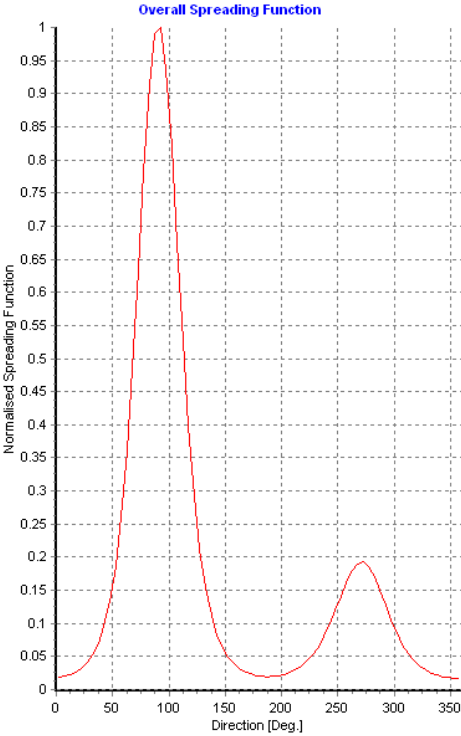


Figure 4.20: Spreading function obtained from Wavelab's, based on test 3.

From the MLM implementation the directional spectra are shown in figure 4.21, 4.22 and 4.23.

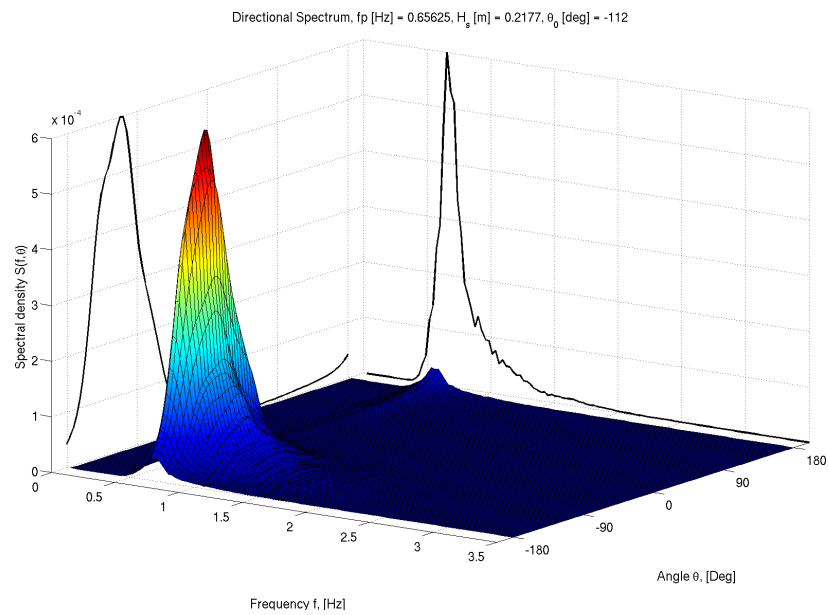


Figure 4.21: Directional spectrum of test 1 obtained from the MLM.

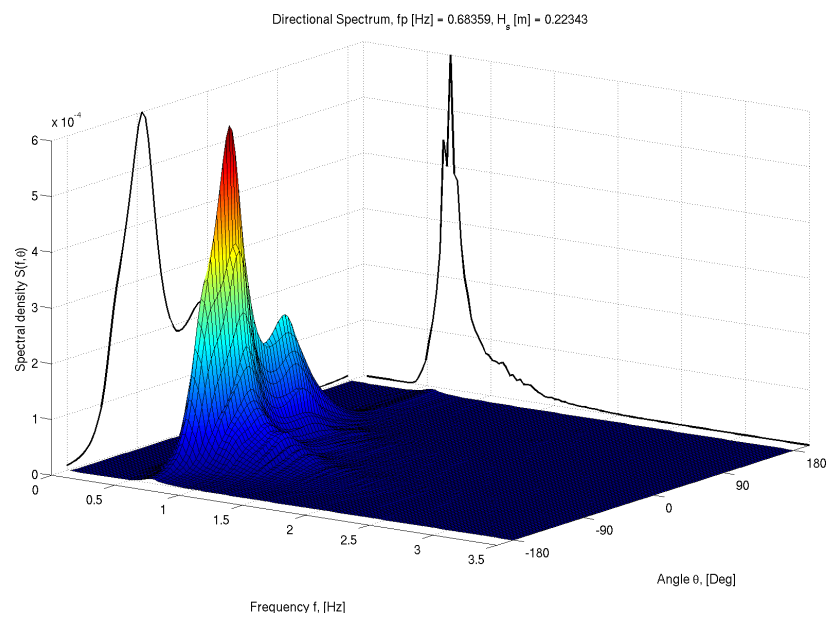


Figure 4.22: Directional spectrum of test 2 obtained from the MLM.

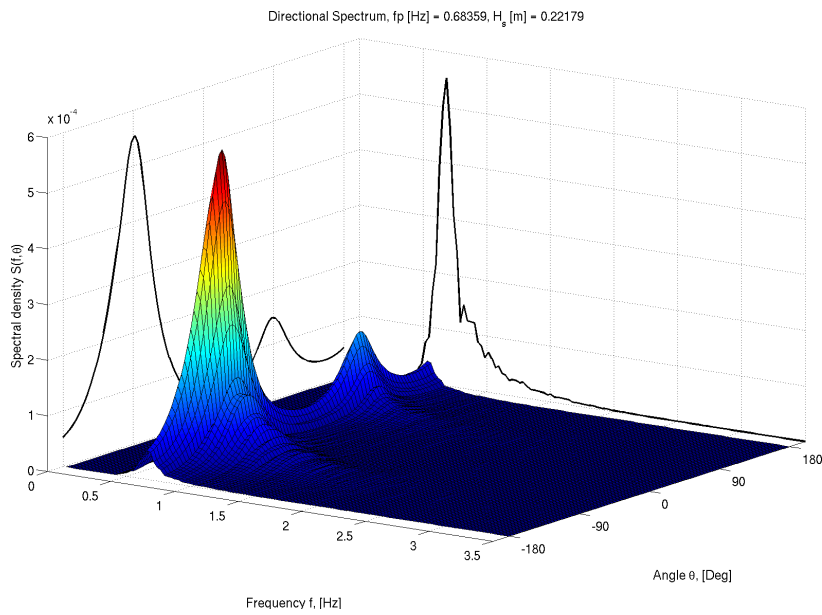


Figure 4.23: Directional spectrum of test 3 obtained from the MLM.

The directional spectra obtained from the MLM implementation appear to fit quite well with the BDM. By manually combining the two spreading functions the similarities can be directly compared in figure 4.24, 4.25 and 4.26.

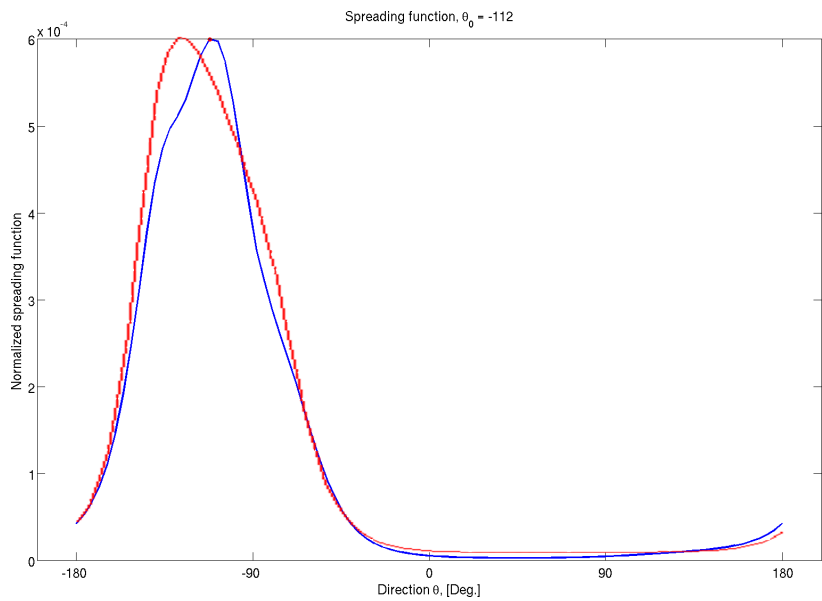


Figure 4.24: Comparison between spreading function of the implemented MLM and the BDM in test 1.

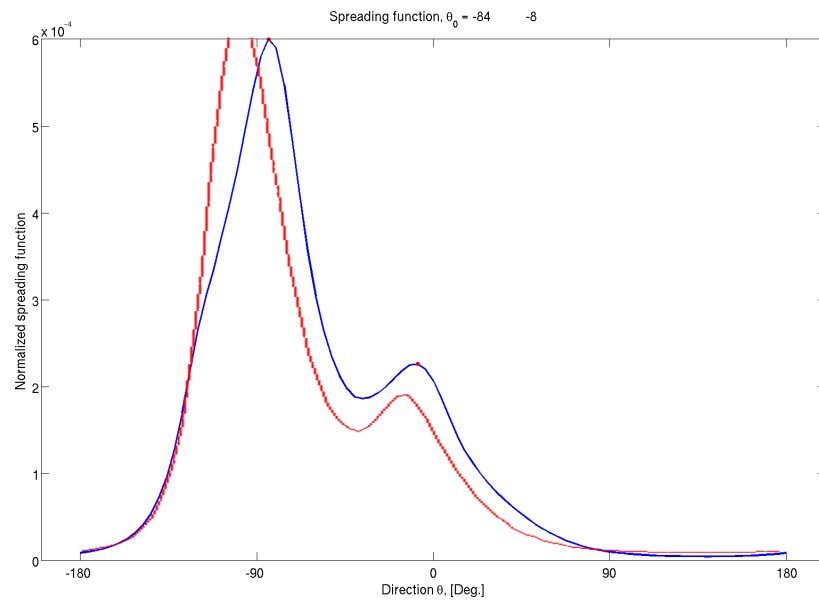


Figure 4.25: Comparison between spreading function of the implemented MLM and the BDM in test 2.

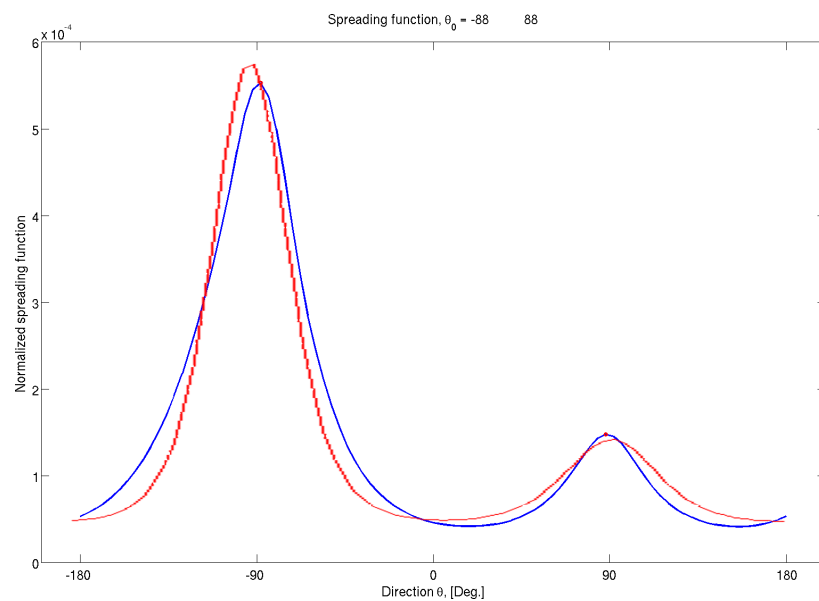


Figure 4.26: Comparison between spreading function of the implemented MLM and the BDM in test 3.

4.4 IAHR wave data

The IAHR wave data are analyzed compared, based on data obtained from Hawkes (1997). The specifications in table 4.6 are from Hawkes et al. (1997). It should be noted that the comparison of the overall mean wave direction, explained in appendix B has not been

implemented due to shortage of time in this project and can therefore not be compared to those found in Hawkes et al. (1997).

| Test | T_p | H_{m0} | θ_0 | θ_{r0} | s | h | Comments |
|------|-------|----------|------------|---------------|-----|------|--|
| A1 | 1.8s | 0.12m | 26 deg. | — | 6 | 3.0m | Standard test |
| A2 | 1.8s | 0.12m | 28 deg. | — | 6 | 3.0m | Double-sum |
| A4 | 1.8s | 0.12m | 25 deg. | — | 6 | 3.0m | 20% noise (all gauges) |
| A5 | 1.8s | 0.12m | 25 deg. | — | 6 | 3.0m | 1.1 gain (η_1 and u) |
| A6 | 1.8s | 0.12m | 25 deg. | — | 6 | 3.0m | Cross talk (η_1/η_2 and u/v) |
| B1 | 1.8s | 0.12m | 29 deg. | — | 40 | 3.0m | Narrow spread |
| C1 | 1.8s | 0.12m | 27 deg. | 126 deg. | 6 | 3.0m | 20% ref., wall par. to wave-maker at 10m |
| C2 | 1.8s | 0.12m | 35 deg. | 139 deg. | 6 | 3.0m | 70% ref., wall par. to wave-maker at 1m |
| C3 | 1.8s | 0.12m | 27 deg. | 151 deg. | 6 | 3.0m | same as C2 but without phase-locking |
| C4 | 1.8s | 0.12m | 20 deg. | 125 deg. | 6 | 3.0m | Cross-resonant modes |
| D1 | 1.8s | 0.12m | 27 deg. | — | 6 | 0.5m | Laboratory basin, “wide spread” |
| E1 | 1.8s | 0.12m | 31 deg. | — | 40 | 0.5m | Laboratory basin, “narrow spread” |

Table 4.6: IAHR wave data specifications based on average values from Hawkes et al. (1997).

Where — means that the parameter is unused.

The results of the implemented MLM analysis and the Wavelab BDM is seen in table 4.7. It should be noticed that while Wavelab (and IAHR) uses the positive x-direction as the 0 degree angle moving counter clockwise, the implementation has the negative x-direction as the 0 degree moving counter clockwise as well. The implemented MLM directions are corrected in the list to resemble IAHR and Wavelab.

| Test | T_p MLM | T_p BDM | H_{m0} MLM | H_{m0} BDM | θ_0 MLM | θ_{r0} MLM | θ_0 BDM | θ_{r0} BDM |
|------|-----------|-----------|--------------|--------------|----------------|-------------------|----------------|-------------------|
| A1 | 1.83s | 1.83s | 0.121 | 0.107 | −4 deg. | — | 37 deg. | — |
| A2 | 1.83s | 1.77s | 0.116 | 0.103 | −4 deg. | — | 39 deg. | — |
| A4 | 1.83s | 1.83s | 0.123 | 0.107 | 4 deg. | — | 37 deg. | — |
| A5 | 1.83s | 1.83s | 0.123 | 0.109 | −12 deg. | — | 37 deg. | — |
| A6 | 1.83s | 1.83s | 0.123 | 0.108 | −12 deg. | — | 36 deg. | — |
| B1 | 1.83s | 1.71s | 0.120 | 0.118 | 0 deg. | — | 30 deg. | — |
| C1 | 1.83s | 1.83s | 0.122 | 0.110 | −4 deg. | 160 deg. | 36 deg. | N/A |
| C2 | 1.83s | 1.77s | 0.136 | 0.121 | 8 deg. | 175 deg. | 60 deg. | N/A |
| C3 | 1.83s | 1.83s | 0.143 | 0.128 | 0 deg. | 179 deg. | 67 deg. | 152 deg. |
| C4 | 1.83s | 1.83s | 0.131 | 0.111 | 0 deg. | 126 deg. | 45 deg. | N/A |
| D1 | 1.83s | 1.83s | 0.118 | 0.107 | 4 deg. | — | 37 deg. | — |
| E1 | 1.83s | 1.83s | 0.119 | 0.118 | 8 deg. | — | 30 deg. | — |

Table 4.7: Analysis of IAHR wave data specifications using MLM implementation and Wavelab’s BDM.

Where *N/A* means that the result is unobtainable.

The MLM implementation is quite inaccurate in determining the peak directions, being off by roughly 30 degrees on both incident and reflected waves. It does appear as if the implemented method is able to distinguish between incident- and reflected- waves in the phase-locking cases of the tests *C1* and *C2*.

Optimization of wave gauge array

The default gauge array used in this project has been the CERC 5 gauge array. The idea of this section is to evaluate alternatives and compare these alternatives to the CERC 5 gauge setup. There are several factors which should be taken into account when comparing these arrays. Of the most important factors are the number of wave gauges used and the results of the analysis utilizing these arrays.

The evaluations in this section breaks down the wave gauge array into separate directions and then some measurement criteria must be established in order to evaluate the gauge arrays against each other. The criteria used are those listed by Goda (2010), they are:

- No pair of wave gauges should have the same vector distance between gauges.
- The vector distance should be distributed uniformly in as wide a range as possible.
- The minimum separation distance between a pair of wave gauges should be less than half of the smallest length of the component waves for which the directional analysis is to be made.

The vector distance referred to is the effective distance in the direction of the waves between two wave gauges. So the vector distance is determined by the wave direction. This can also be explained by introducing a co-array defined in lag-space which is based on Davis and Regier (1977). This means that the latency from when a wave reaches the first gauge in a gauge pair till it reaches the second is used. The idea is to optimize the gauge placement to increase the number of elements in the co-array without sacrificing the uniformity of the array as this will limit side-lobe leakage due to a better resolution and thereby improve the accuracy of the directional spectrum.

To explain how this co-array may help determine the better wave gauge array, three simple line-arrays are used in figure 5.1.

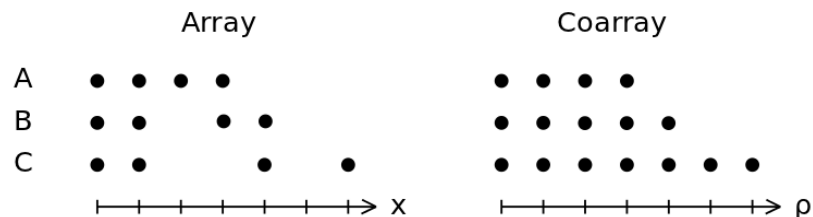


Figure 5.1: Arrays and co-arrays of three different line arrays.

A is a simple array with evenly spaced gauges while B and C are distributed as suggested by Pawka (1974) and Barber (1963) respectively. From this example it is seen that C has the largest number of distinctive lags and are furthermore uniformly distributed.

The second criterion defines the highest frequencies which are unaffected by aliasing obtained in the cross-spectra. It is written as equation (5.1).

$$l_G < L/2 \quad (5.1)$$

Where l_G is the gauge distance and L is the wavelength. By fulfilling this expression it is shown by Barber and Doyle (1956) that the phase difference, Ψ is within the limits $-\pi \leq \Psi \leq \pi$.

The wave-direction directly affects the vector distance and thereby also the extent of the co-array. So in order to keep the resolution and accuracy of the directional spectrum high it is necessary to include some redundancy in various directions. Ideally these redundancies should be placed uniformly¹. This can be seen to be fulfilled quite well in the standard CERC 5 gauge array, in this example with the default minimum gauge pair distance is 0.2m. The array is shown in figure 5.2. As seen the CERC array got three unique distances, in this case they are 0.200m, 0.235m and 0.380m.

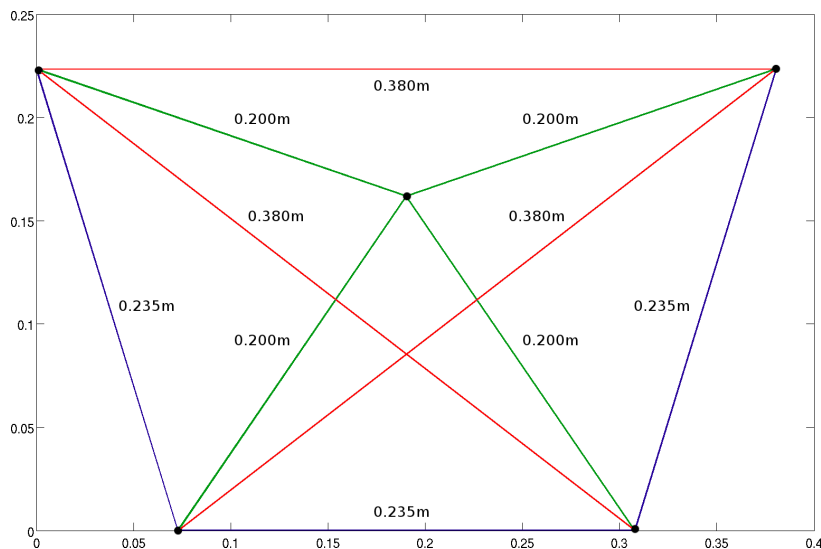


Figure 5.2: CERC 5 gauge array.

In order to streamline the evaluation a script is created which calculates the vector distances between each gauge pair for a discrete set of directions. Using the criteria defined above the maximum distance and the number of distinctive distances are used to determine the weaknesses. The Co-array of the vector distances are calculated for the CERC 5 gauge array in figure 5.3.

¹In example: Three redundancies could be placed at the angles 0 deg. 60 deg. 120 deg.

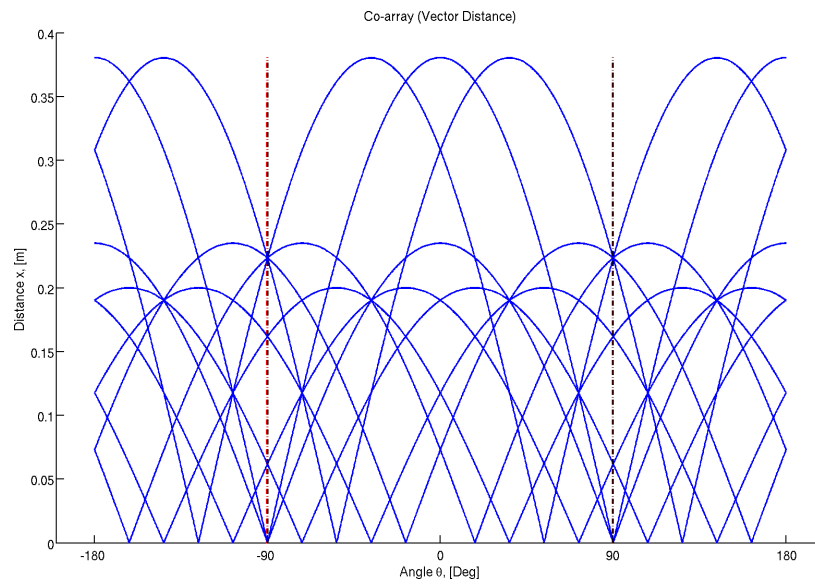


Figure 5.3: Vector distances in the CERC 5 gauge array.

Where the blue lines are the vector distances of all available gauge pairs. The black and red dashed lines are coinciding in the same locations. The black line indicates the direction with the least amount of elements in the co-array and the red line is the directions with the shortest co-array.

This can then be illustrated by combining directions with the array, as seen in figure 5.4. From the co-array it is seen that the likely weakness is waves coming straight at the array. The largest separation of gauges are 0.22m which, compared to 0.38m for most other directions is a large difference. The minimal number of unique vector distances are three shown at the red lines.

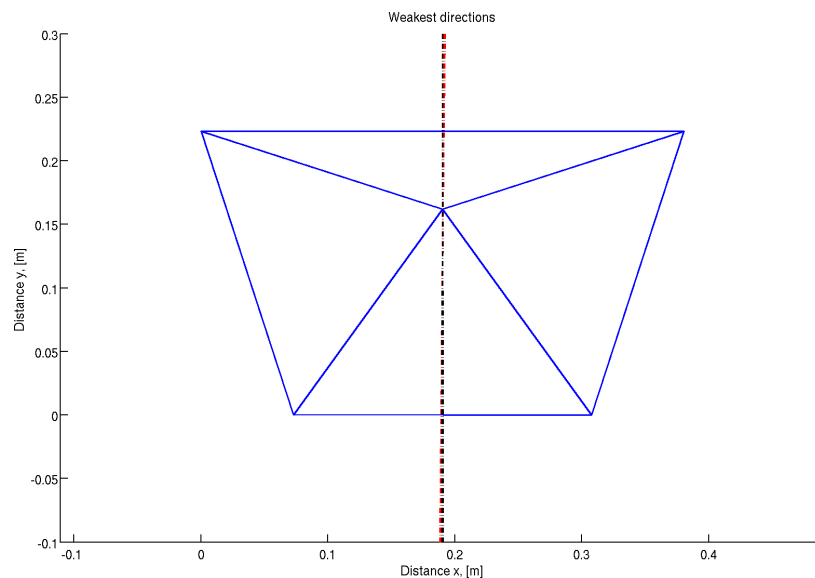


Figure 5.4: Expected weaknesses of the CERC 5 gauge array.

An alternative to the CERC array is the Haubrich (1968) array with six gauges placed on the sides of a triangle as illustrated in figure 5.5.

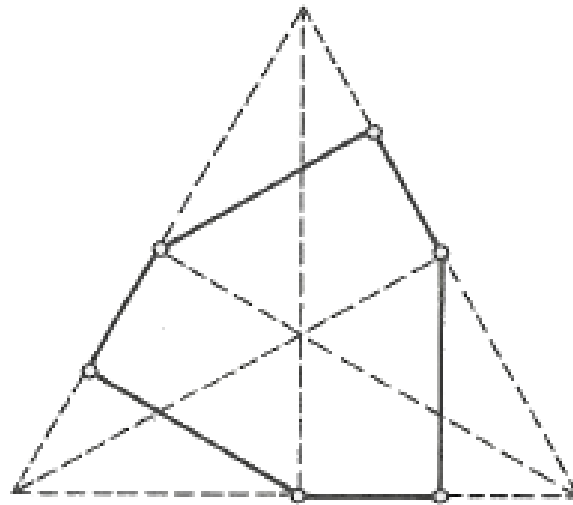


Figure 5.5: Haubrich's array, figure from Goda (2010).

Using the minimum gauge pair distance of 0.2m as in the CERC array, the corresponding tests are shown in figure 5.6 and figure 5.7.

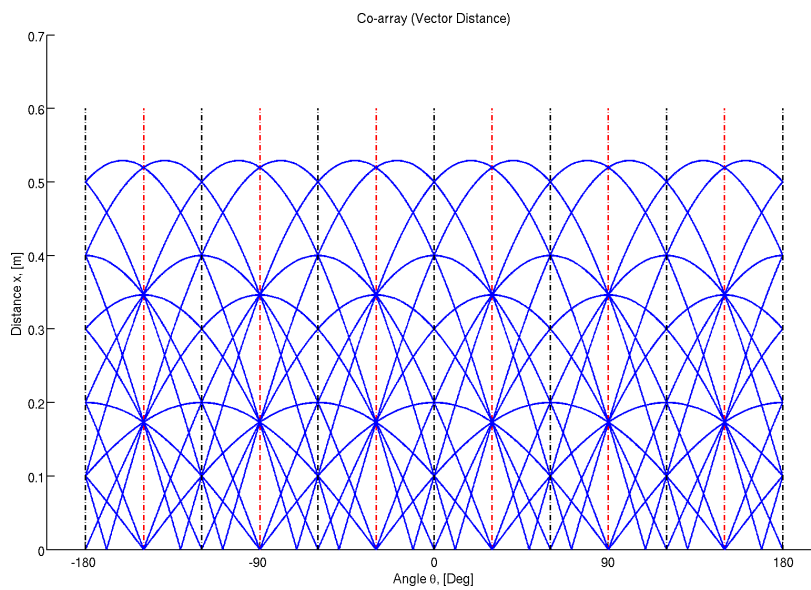


Figure 5.6: Vector distances in the HAUB 6 gauge array.

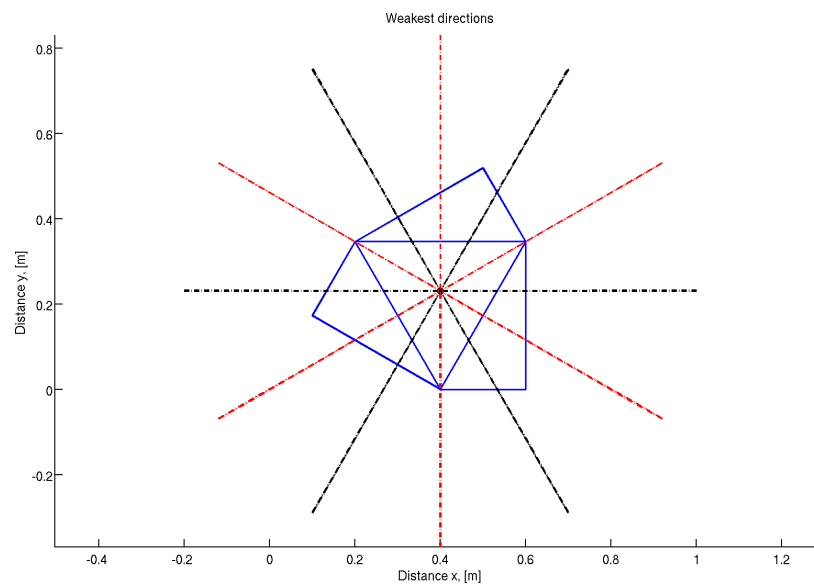


Figure 5.7: Expected weaknesses of the HAUB 6 gauge array.

In this array the largest difference when comparing the separation of gauges are from 0.50m at the weakest point to 0.53m at the strongest equal to a difference of 6%. The minimal number of unique vector distances are three like the CERC array.

The final array tested is the 6 gauge array where one additional node is added to the top on the circle of the CERC-5 gauge array. This array is used in the IAHR project, Hawkes (1997). The results are seen in figure 5.8 and figure 5.9.

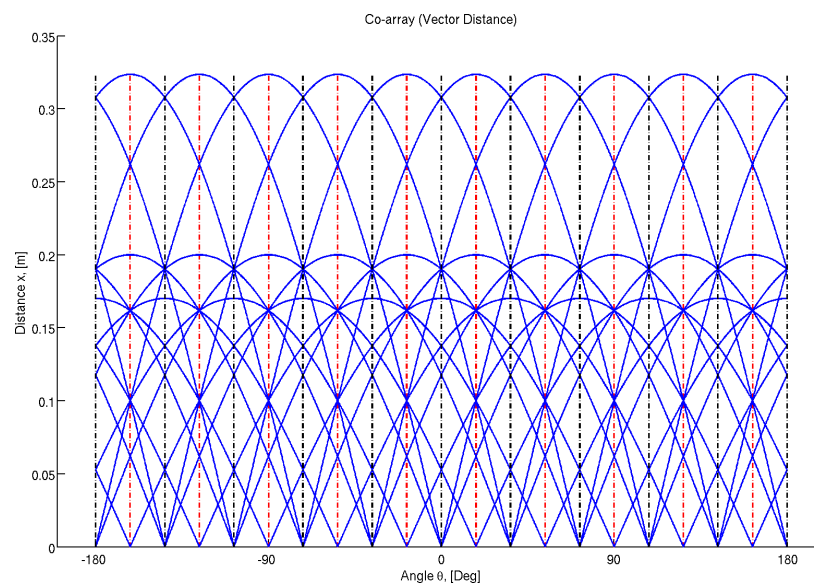


Figure 5.8: Vector distances in the modified 6 gauge CERC array.

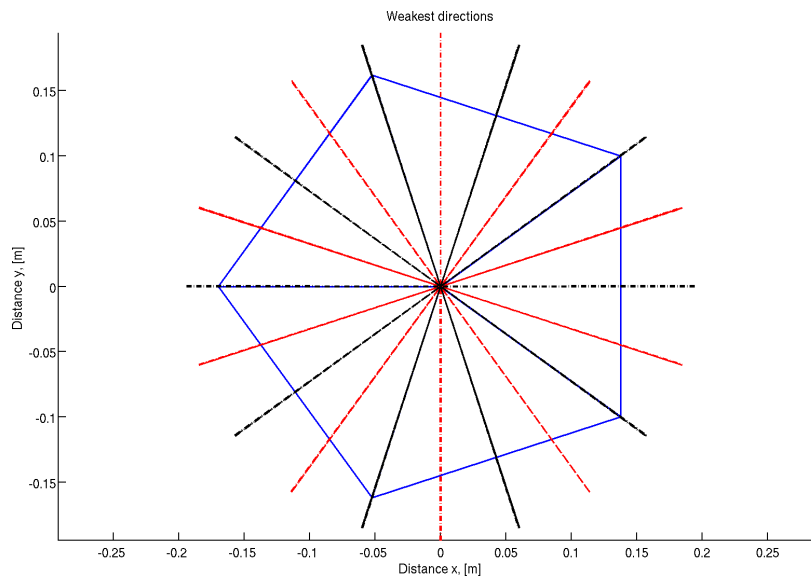


Figure 5.9: Expected weaknesses of the modified 6 gauge CERC array.

Comparing the maximal vector distance between the weakest and strongest point in the array equals to a difference of 5% and with six unique vector distances as minimum this method appears to be superior based on the chosen criteria.

Overall the 6-gauge arrays should produce more stable results regardless of the direction. This method is meant to be supported or rejected by extensive testing, where high and low frequency waves is sent uni-directionally in various directions and then comparing the results with the specifications of the co-arrays. Due to shortage of time this is not possible though.

Conclusion

Through the progression of creating this report the generating methods has been of increasing importance, particularly because of the ability to queue tests using any of the implemented methods and specifying which parameters to use. This has allowed for very extensive testing with no user involvement while the scripts works through uni-directional, unimodal and/or bimodal wave generations and directly analyzing these generated waves using the implemented Maximum Likelihood Method. Additionally all relevant data are automatically put into timestamped files, including figures, wave properties and comparisons between the expected generated models and the models found through analysis. So while important tests have been performed using waves generated in Wavelab and obtained from the IAHR database the most extensive testing has been performed using the methods implemented. So it has been important to ensure that the implemented methods works as intended. To do so the Bayesian Deterministic Method used in Wavelab and the MLM implemented in DIWASP has been used to verify the generated data. All generating methods appears to work as intended with the exception of the reflection parameter, which has been reported by Wavelab to be too large for the generated waves.

The implemented methods are using the superposition of regular waves to generate irregular waves. The advantage of using this generating method is that it is intuitive. There is also a clear progression from the uni-directional wave generation all the way to the bimodal wave generation. The drawback is the execution time which is considerably slower than for instance the phase difference method.

The implemented analysis has been the most time-consuming part of this project. Particularly the attempt of making implementation of the piecewise constant method work. Extensive bug-searching of each individual part of the script has been performed and large parts of the script was entirely rewritten and even replaced later by parts of the well-working MLM. But no matter what was done the results where unsatisfying.

The MLM was the second method implemented, remarkably this method was surprisingly easy to implement and it took only a few days before it returned realistic results. The calculation of the directional spectra and spreading function in the MLM only takes a few seconds, and the results obtained from this method are quite satisfying. Both waves generated from the implemented methods and from Wavelab produces good results but also most of the IAHR tests are quite accurate although the directions of the peaks are off. The implemented MLM even managed to obtain reasonable results from the bimodal test case $C1 - C4$ and bimodal tests performed in Wavelab. This may be happenstance though as the method does not include functionality to account for the relation between the phase of the incident and reflected waves.

Isobe introduced a modification to the MLM. This method should account for the relation between the incident and reflected phase by including a reflected wave gauge array, which is a function of the location of the reflection line. Up to this point the implemented method seems to work. But as the location of the reflection line is difficult to determine in real cases, the idea is to find this by letting the program determine the parameters for the line. This introduces a problem as it is unclear what criteria should be used to determine when the right distance and direction is found.

The wave gauge array used in this project is based on the CERC 5 gauge array. To compare this array with other arrays it is necessary to determine which criteria should be taken into account. In this report the focus is on the actual vector distances between gauge pairs based on the direction of the wave trains. The quality of the array is then defined by the number of unique vector distances in the array, the uniformity of the distribution of the vector distances and the maximal vector distance available at the any given direction. The array which fit these criteria the best should have the better resolution and thereby improve the accuracy of the directional spectrum. Through this test the weaknesses are then found in the gauge array and it is then possible to run extensive testing on the given direction(s). Using this method to evaluate the CERC 5 gauge array it was clear than the CERC 5 gauge array may have a weakness when waves approach straight at it. Two other wave gauge arrays were then tested, both consisting of 6 gauges. One similar to the CERC 5 gauge array but with an additional wave gauge forming a pentagon with one central node and one by Haubrich (1968), which is based on a triangle with nodes on the sides. Both of these gauge arrays has a better distribution of the vector distances when considering waves from an arbitrary direction. But with a minimum of six distinct vector distances the modified CERC array would seem like the better choice, even though the extent of the vector distances were narrower.

Appendices

Spectral estimation

The procedure used to estimate the spectral density functions from sample functions, referred to here as the spectral estimation, is primarily based on Bendat and Piersol (2000), a fundamental explanation of the spectral density function is explained in appendix E.1.

The method used to determine the spectral density functions is via finite Fourier Transforms of the sample functions. In this project is required that the sample functions $\eta_x(t)$ and $\eta_y(t)$ defined in the limited time interval $0 \leq t \leq T$ must be part of associated stationary random processes¹.

Through Fourier Transformation a spectral density function are obtained by equation (A.1), with the Fourier Transform $X(f, T)$.

$$\Phi_{(2sided),xy}(f, T) = \frac{1}{T}X^*(f, T)Y(f, T), \quad -\infty < f < \infty \quad (\text{A.1})$$

$$(\text{A.2})$$

The spectral density function in equation (A.1) is double-sided spectrum mirrored at the the zero-frequency (and again in the Nyquist frequency). For the purposes in this project the negative frequencies are not needed and instead a one-sided spectrum in equation (A.3) is used and multiplied by two to preserve the energy.

$$\Phi_{xy}(f, T) = \begin{cases} \frac{2}{T}X^*(f, T)Y(f, T) & 0 \leq f < \infty \\ 0 & -\infty < f < 0 \end{cases} \quad (\text{A.3})$$

By expansion equation (A.3) may be written as equation (A.4).

$$\begin{aligned} \Phi_{xy}(f) &= C_{xy} - iQ_{xy} \\ \text{where :} \\ C_{xy} &= \frac{2}{T}(\Re(X)\Re(Y) + \Im(X)\Im(Y)) \\ Q_{xy} &= \frac{2}{T}(\Re(X)\Im(Y) - \Im(X)\Re(Y)) \end{aligned} \quad (\text{A.4})$$

As C_{xy} and Q_{xy} are the coincident- and quadrature-spectral density functions respectfully of the Fourier Transforms $X(f, T)$ and $Y(f, T)$. For convenience these two functions are referred to later as co- and quad-spectra.

The Fourier Transform of the sample functions $\eta_x(t)$ and $\eta_y(t)$ are defined by equation (A.5)

¹Stationarity implies that statistical parameters such as the mean, correlation and covariance may be determined from a sample function in a limited time-span.

$$\begin{aligned} X(f, T) &= \int_0^T \eta_x(t) e^{-j2\pi ft} dt \\ Y(f, T) &= \int_0^T \eta_y(t) e^{-j2\pi ft} dt \end{aligned} \quad (\text{A.5})$$

The Discrete Fourier Transform, DFT, of equation (A.5) is written as equation (A.6).

$$X(f, T) = \sum_t^T \eta_x(t) \exp(-j2\pi ft) \Delta t \quad (\text{A.6})$$

To improve calculation time (from $O(N^2)$ to $O(N \log N)$) the Fast Fourier Transformation, FFT, is used instead of the DFT. The FFT requires that the block size is of a power of two, to ensure this condition is satisfied the sample functions are divided into B blocks of size b which leads to equation (A.7).

$$X_b(f, T, b) = \sum_{n=0}^{N-1} \eta_n(t) \exp\left(-j \frac{2\pi f b n}{N}\right) \Delta t, \quad b = 1, 1, 2, \dots, B \quad (\text{A.7})$$

To handle sample functions of arbitrary sizes it is chosen to fill the last block with trailing zeros. The spectral matrix are then calculated by the estimate of the B blocks, assuming that the time interval T is large enough to obtain a representative sample.

$$\Phi_{xy}(f) = \lim_{T \rightarrow \infty} E[\Phi_{xy}(f, T, b)] \quad (\text{A.8})$$

A.1 Improvement of estimate

The procedure which are implemented are the one suggested by Bendat and Piersol (2000, section 11.5.3) where the ensemble-averaged auto-spectral density estimates are computed.

In order to suppress side-lobe leakage the data blocks are each tapered with the Hanning tapering window, where the loss generated by the tapering window is determined by the difference in covariance before and after the tapering. The trade-off when using this method is that the tapering windows also increases the main lobe of the spectral window. Compensating for this can be done by either creating overlapping blocks or simply obtaining a longer record. In this project a 50% overlapping of the blocks are used as suggested by the literature.

A.2 Unidirectional spectral estimation

In the case of unidirectional wave trains the one-sided spectral density function is rewritten to equation (A.9).

$$\Phi_{xx}(f) = \begin{cases} \frac{2}{T}|X(f,T)|^2 & 0 \leq f < \infty \\ 0 & -\infty < f < 0 \end{cases} \quad (\text{A.9})$$

A.3 The frequency spectrum

The Jonswap spectrum has a high concentration of energy compared to the predecessor, the Pierson-Moskowitz spectrum, Mitsuyasu et al. (1975), suggested to use Jonswap for wind dominated waves, while using PM for swell. Furthermore US. Army engineer corpse suggests in a technical note, U.S. Army Engineer (1985a), to use the TMA spectrum Hughes (1984) for shallow water cases, which is a further development of the Jonswap spectrum to incorporate the water depth.

Cosine squared distribution

The cosine squared distribution was introduced by Longuet-Higgins et al. (1963). It is defined by equation (B.1).

$$D(\theta) = G'(s) \cdot \left| \cos \left(\frac{\theta - \theta_0}{2} \right) \right|^{2s} \quad (\text{B.1})$$

Where s is a spread parameter and θ_0 is the main direction of the waves.

The spreading function can be defined either as a real or positive function depending on the literature, in the original work by Longuet-Higgins et al. (1963) the cosine squared distribution is a positive function, which is shown in equation (B.1). $G'(s)$ is a function used to normalize the cosine expression to satisfy equation (B.2).

$$\int_{-\pi}^{\pi} D(\theta) d\theta = \pi \quad (\text{B.2})$$

$G'(s)$ is calculated by equation (B.3).

$$G'(s) = 2^{2s-1} \frac{\Gamma^2(s+1)}{\Gamma(2s+1)} \quad (\text{B.3})$$

Where Γ is the gamma function. Due to the definition of the relationship between the one-dimensional spectrum, the directional spectrum and the spreading function in section 3.1 the spreading function should be normalized to one instead leading to equation (B.4) and equation (B.5).

$$\int_{-\pi}^{\pi} D(\theta) d\theta = 1 \quad (\text{B.4})$$

$$D(f, \theta) = \frac{2^{2s-1}}{\pi} \frac{\Gamma^2(s+1)}{\Gamma(2s+1)} \cos^{2s} \left(\frac{\theta - \theta_0}{2} \right) \quad (\text{B.5})$$

Where denoting the spreading function as a function of the frequency serves as a reminder of the connection between the spread parameter and the frequency, which is used in section B.1.

The relation between the spreading function and the spread parameter may be visually interpreted by figure B.1.

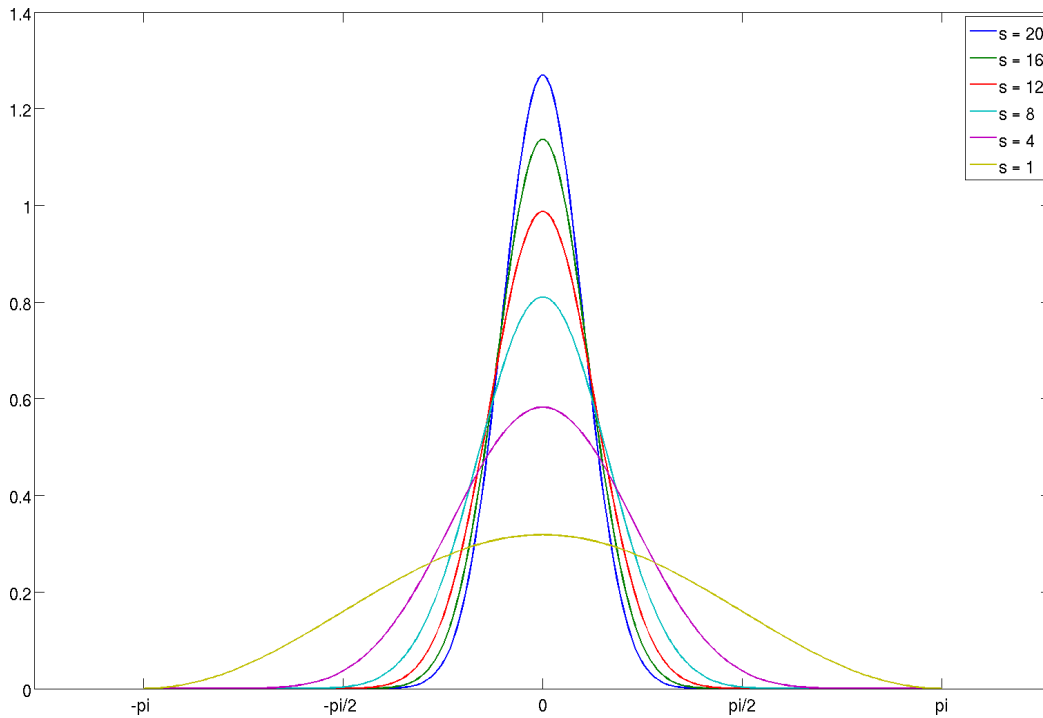


Figure B.1: Visual interpretation of the spreading function and the spread parameter.

B.1 The frequency dependent spread parameter

To determine the value of the spread parameter Goda (1999) suggests to use an expression for s formulated by Mitsuyasu et al. (1975) as seen in equation (B.6).

$$s = \begin{cases} s_{max}(f/f_p)^5 & f \leq f_p \\ s_{max}(f/f_p)^{-2.5} & f > f_p \end{cases} \quad (\text{B.6})$$

Where s_{max} is determined by the type of waves, low values for wind waves and high values for swell waves with long decay distance.

B.2 Spreading function comparison

In order to compare spreading functions which are not only modeled by the cosine squared function it is necessary to have a parameter which defines the degree of the spread of D .

One method is using the directional spreading σ_θ defined by Frigaard et al. (1997). The method suggested takes into account the discrete computation of waves which can cause incorrect results when analyzing bimodal waves. The peak direction θ_0 and the directional

spreading σ_θ are defined by equation (B.7) and equation (B.8).

$$\theta_0 = \text{atan}(c_1) \quad (\text{B.7})$$

$$\sigma_\theta = \sqrt{2(1 - |c_1|)} \quad (\text{B.8})$$

$$c_1 = \int_0^{2\pi} D(f, \theta) \cos(\theta) d\theta + i \int_0^{2\pi} D(f, \theta) \sin(\theta) d\theta$$

The relation between the directional spreading and the spread parameter of the cosine squared method is illustrated by figure B.2.

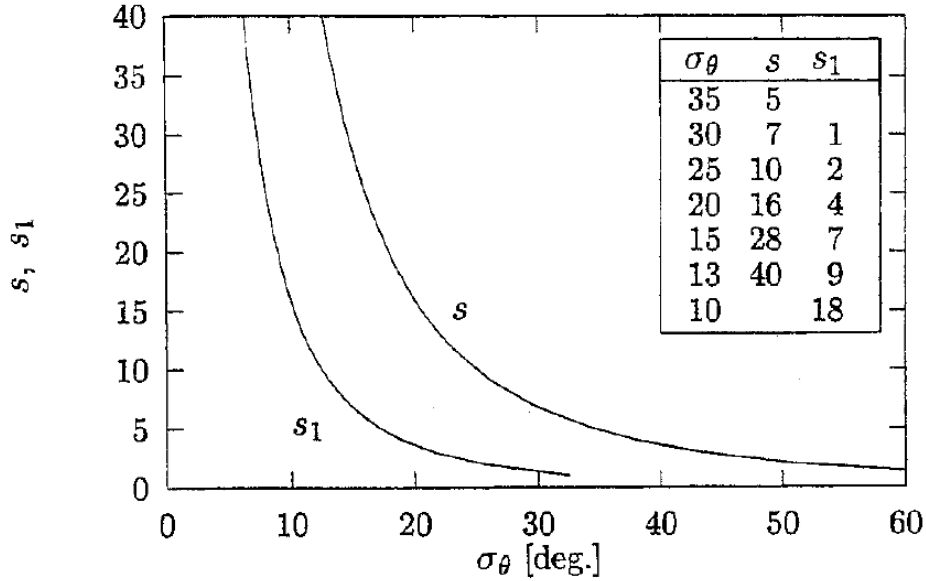


Figure B.2: Relation between the spread parameter s and the standard deviation σ . The figure is from Frigaard et al. (1997).

Where s_1 is an alternative to the traditional cosine squared method in equation (B.5). This alternative is shown in equation (B.9).

$$D(f, \theta) = \frac{1}{\sqrt{\pi}} \frac{\Gamma(s_1 + 1)}{\Gamma(s_1 + 1/2)} \cos^{2s_1}(\theta - \theta_0) \quad (\text{B.9})$$

Hawkes et al. (1997) has used this method to compare a wide range of wave analysis methods. The data used for the comparison are from the IAHR project, Hawkes (1997), which are also the wave data used in the comparison section 4.4 of this report. The exact comparison criteria is the overall mean wave direction $\underline{\sigma}$ shown in equation (B.10).

$$\underline{\sigma} = \frac{\int \sigma_\theta(f) S(f) df}{\int S(f) df} \quad (\text{B.10})$$

Maximum likelihood method

This explanation covers two aspects, the first being the theory of the MLM, the second being the actual implementation.

C.1 Theory

The description of the general Maximum Likelihood Method, MLM, is explained based on Davis and Regier (1977) and Isobe and Kondo (1984), with support from Isobe et al. (1984), Benoit et al. (1997), Ayyub and McCuen (2002), Ochi (1998) and Scott and Nowak (2004). The intent is to end up explaining the MLM and MMLM methods used in section 3.5.

As hinted by the name the method maximizes the probability of obtaining a particular sample, this is done by determining the global maximum of the likelihood function. The peak may be obtained by differentiating the likelihood function and finding the zero crossing(s), in case of multiple peaks the global maximum should be used. The function is written as equation (C.1).

$$\frac{d\ln(L(\lambda))}{d\lambda} = 0 \quad (\text{C.1})$$

λ being the parameter.

Equivalently to obtaining the maximum likelihood estimate is to minimize the error in the variance estimate. This however requires that the processing method is constrained to unit gain when there is no noise on the signal. Since it is the variance of the signal which is the most relevant in the case of spectral estimation, it is the approach used by Davis and Regier (1977) and hence subsequently by Isobe et al. (1984).

The central aspect of the method is the estimated wavenumber-frequency spectrum defined by equation (C.2).

$$\hat{D}(\mathbf{k}, \theta) = \sum_{n,m} \alpha_{nm}(\mathbf{k}, \theta) \Phi_{nm}(\theta) \quad (\text{C.2})$$

Where $\sum_{n,m}$ is a summation of n and a summation of m , α_{nm} is a weighting of the cross spectra defined in equation (C.3).

$$\alpha_{nm}(\mathbf{k}, \theta) = \gamma_m(\mathbf{k}, \theta) \gamma_n^*(\mathbf{k}, \theta) = e^{-i\mathbf{k}(x_n - x_m)} \quad (\text{C.3})$$

Φ_{nm} is the cross spectra, equation (C.4), defined similarly to equation (3.12) and (3.13) used in the discrete method.

$$\Phi_{nm}(\theta) = \int_{\mathbf{k}} e^{-i\mathbf{k}(x_n-x_m)} D(\mathbf{k}, \theta) d\mathbf{k} \quad (\text{C.4})$$

By insertion of equation (C.4) into equation (C.2) the expression reads

$$\hat{D}(\mathbf{k}, \theta) = \sum_{n,m} \alpha_{nm}(\mathbf{k}, \theta) \int_{\mathbf{k}} e^{-i\mathbf{k}(x_n-x_m)} D(\mathbf{k}, \theta) d\mathbf{k} \quad (\text{C.5})$$

By introducing the window-function W and dividing the wavenumbers into an integrated \mathbf{k}' and un-integrated \mathbf{k} .

$$\hat{D}(\mathbf{k}, \theta) = \sum_{n,m} \alpha_{nm}(\mathbf{k}, \theta) \int_{\mathbf{k}'} e^{-i\mathbf{k}'(x_n-x_m)} D(\mathbf{k}', \theta) d\mathbf{k}' \quad (\text{C.6})$$

The expression can be rewritten as equation (C.7).

$$\hat{D}(\mathbf{k}, \theta) = \int_{\mathbf{k}'} D(\mathbf{k}', \theta) W(\mathbf{k}, \mathbf{k}') d\mathbf{k}' \quad (\text{C.7})$$

where W is defined by equation (C.8).

$$W(\mathbf{k}, \mathbf{k}') = \sum_{n,m} \alpha_{nm}(\mathbf{k}, \theta) e^{-i\mathbf{k}'(x_n-x_m)} \quad (\text{C.8})$$

by inserting equation (C.3) into equation (C.8) the expression can be rewritten to equation (C.9) .

$$W(\mathbf{k}, \mathbf{k}') = \sum_{n,m} \gamma_m(\mathbf{k}, \theta) \gamma_n^*(\mathbf{k}, \theta) e^{-i\mathbf{k}'(x_n-x_m)} \quad (\text{C.9})$$

The wavenumber frequency spectra are of the best resolution when the window function W approximates to a Dirac delta-function at $\mathbf{k} = \mathbf{k}'$. This leads to equation (C.10).

$$W(\mathbf{k}, \mathbf{k}') = \left| \sum_m \gamma_m(\mathbf{k}, \theta) e^{-i\mathbf{k}'(x_m)} \right|^2 \quad (\text{C.10})$$

Then applying the imposed constrain of unit gain, the expression should fulfill equation (C.11).

$$\sum_{m,n}^M W(\mathbf{k}, \mathbf{k}') = 1 \quad (\text{C.11})$$

And so by combining equation (C.10) (C.11) and (C.3) the expression of the estimated wavenumber-frequency spectrum defined in equation (C.2) can be rewritten as equation (C.12).

$$\hat{D}(\mathbf{k}, \theta) = \kappa / \left[\sum_{m,n}^M \Phi_{nm}^{-1}(\theta) e^{i\mathbf{k}(x_n - x_m)} \right] \quad (\text{C.12})$$

Where κ is a proportionality constant which is determined from the relationship between the wavenumber frequency spectrum and the power spectrum.

The structure of the implementation

The reason for choosing Matlab as the implementation environment is primarily due to the large collection of toolboxes available within the environment. The tools are used to focus the attention on what is relevant for the project and not on time consuming off-topic functionality. In this chapter the entire implementation made in this project is outlined. For a more in-depth view into the implementation it is suggested to look through the code in the *Implementation* section of the DVD. Comments and explanations are left in the code for this purpose. In this appendix it is assumed that the main report has been read beforehand, as terminology and references are implicit.

The folder structure used for this implementation is illustrated in figure D.1.

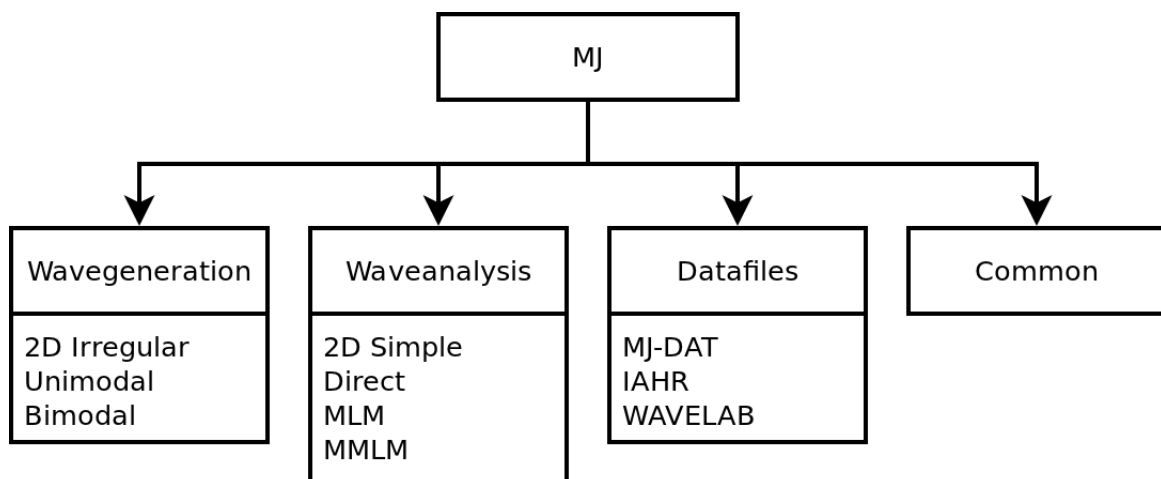


Figure D.1: Folder structure and main functions.

Notice that *Wavegeneration* and *Waveanalysis* have separate subfolders and that these subfolders contain all the implemented methods. Furthermore a *Datafiles* folder is used to store the datasets divided into generated datafiles from this implementation, IAHR and WAVE-LAB. The last folder named *common* is a folder containing scripts which are essential to the implementations but at the same time uninteresting to review, functions such as import of

Wavelab and IAHR files are found here along with scripts handling plotting of graphs and surfaces.

D.1 The main files

Files named *main.m* or *main_auto.m* are meant as the user access points. These files can be run directly and only parameters in these files should be modified. In *main.m* all parameters are set directly in the file, while *main_auto.m* uses a script file which are specified inside *main_auto.m*. The purpose of the auto-script is that consecutive setups can be executed sequential without user-interaction. Concretely speaking the auto-script in the main *Implementation* folder is used to firstly generate waves with properties specified in the script file then save the directional spectrum plot and wave properties to files along with the data series. Secondly it initiates the Maximum likelihood analysis and computes the directional spectrum, which again is saved along with the analyzed wave properties. These data are be found in *Datafiles* under *MJ-dat* ordered by a auto-generated time stamp, an example is shown in figure D.2, where all files belong to one wave generation and analysis.

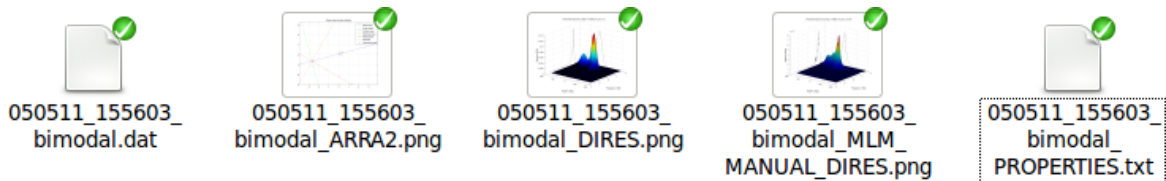


Figure D.2: Auto generated files, including directional spectrum plot, wave properties and the time series.

From left to right the files are the data file containing the time series in the Wavelab format. Three picturefiles containing the wavegauge array, the generated wave series directional spectrum and the analyzed spectrum respectfully. Finally the text file contains the two groups of properties, the generated and the analyzed, illustrated in figure D.3. This text-file can be used for comparison and to reproduce waves with the same properties later.

The script-file must be formatted in a strict way in the sense that the parameters must come in the right order and separated by taps only. The number of taps used between the parameters are disregarded in the evaluation of the script however, and this may be used to properly place parameters above and below each other. An example utilizing all available generation methods is shown in figure D.4. As seen the different generation methods uses a different combination of parameters. To keep the script file easily manageable a header is added specifying in which order the parameters should be placed.

The explanation of the parameters are also found in *main_auto*. The *time* parameter is the length of the sample in seconds, *nf* is the number of frequencies to divide the spectrum into, *wp* is the wave plots to be performed see *main_auto* for the plot number correspondence. *ar.tp* and *ar.sz* are array type and array size where *ar.tp* = 1 and *ar.sz* = 0.2 correspond to a CERC array with the minimal distance from wave gauge to wave gauge of 0.2 m. *r* is the

```

-----
GENERATION
-----
Tp = 1.5
Hs = 0.2
h = 0.6
nth = 41
th0 = 0.2618
s_0 = 15 7
r = 0.5
m_th = -0.5236
m_d = -3
time = 5400
nf = 256
arraytype = 1
arraysize = 0.2
noicelevel = 0.1
-----
ANALYSIS
-----
fp = 0.68359
th0 = 0.29836      1.9481
Hs = 0.30151
r = 1.7757+6.5413e-06i
x = 0      0.37958      0.18979      0.073592      0.30599
y = 0.22465      0.22465      0.16268      0      0
h = 0.6
nfft = 256
method = MLM

```

Figure D.3: Waveproperties obtained from properties-textfiles generated by *main.m* and *main_auto.m*.

```

MJ_Autogeneration_script
-----
Generation type | Tp | Hs | h | time | nf | x | wp
-----
unimodal      1.5 | 0.2 | 0.6 | 54 | 256 |   | [0 0 0 0 0 0 1]
bimodal2     1.5 | 0.2 | 0.6 | 540 | 256 |   | [0 0 0 0 0 0 0 1]
bimodal      1.5 | 0.2 | 0.6 | 540 | 256 |   | [0 0 0 0 0 0 1]
simple2D      1.5 | 0.2 | 0.6 | 5400 | 256 | [0 10] | [1 1]
unimodal     1.5 | 0.2 | 0.6 | 540 | 256 |   | [0 0 0 0 0 0 1]

| save | noice | nth | th0 | s_0 | ar.tp | ar.sz | r | m_th | m_d
-----
[1 1] 0.1 41 0 12 1 0.2
[1 1] 0.1 11 0 [12 7] 1 0.2 0.5 -0.5236 -1
[1 1] 0.1 11 [0 .3] [12 7] 1 0.2 0.5
1
[1 1] 0.1 11 0 12 1 0.2

```

Figure D.4: Example script-file containing an all available generation methods and the corresponding properties.

reflection coefficient and finally m_th and m_d are direction and distance of the mirror line in the bimodal wave generation case.

D.2 Wave generation

The three generation types shown in figure D.1, are the unidirectional irregular waves and multi-directional waves with one main peak called unimodal and with two main peaks called

bimodal. Three other cases are kept separate from these three general generation types. The first case is in the unidirectional wave generation, where the random phase method was tested. The second is in the unimodal case where an experiment has been made where the calculation of the elevation is done in a complete field, by which a water surface is created. The third is in bimodal wave generation where two approaches are available, the primary method is the case with one peak direction and a reflection line and the secondary method is the one handling bimodal waves with two peak directions defined in the properties.

In the following only the three main generation types are used. These three methods are named *simple2D.m*, *unimodal.m* and *bimodal2.m* respectively. To obtain a good structure in the implementation it is sought to ensure that each script has only one major functionality. This means that the three methods only serves as backbones and to a great extend utilizing common scripts. This is clearly shown in figure D.5 which shows which scripts the three methods uses.

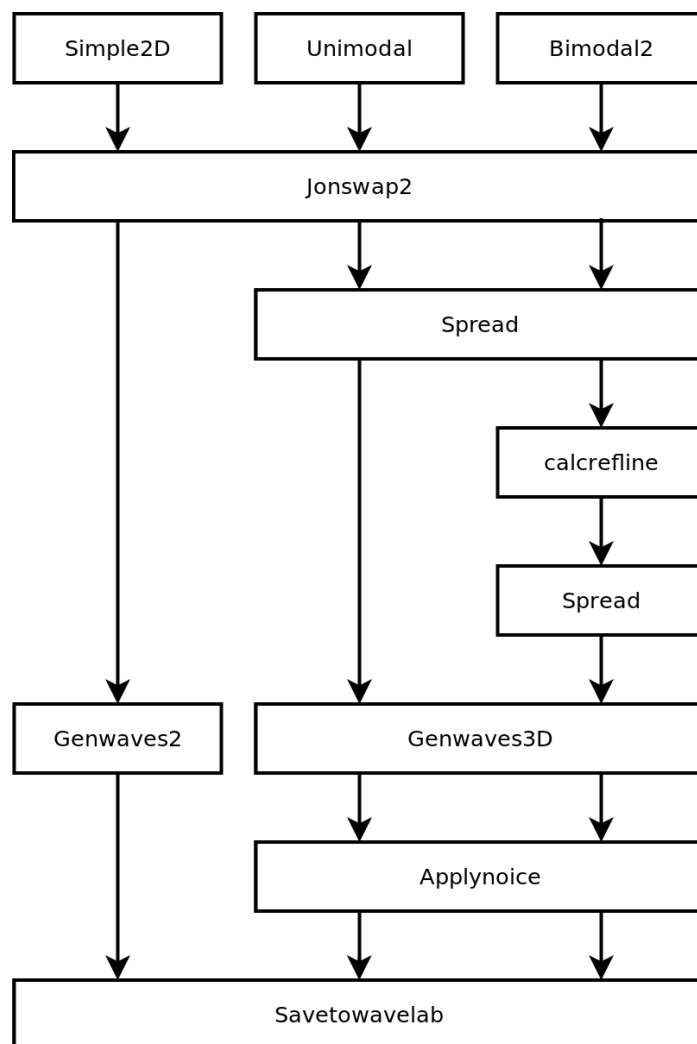


Figure D.5: Scripts used for wavegeneration.

Where *Jonswap2* is the second implementation of the Jonswap spectrum which uses the implementation by Goda (1988). *Spread* is the spreading function based on Mitsuyasu et al.

(1975). *Calcrefline* is used to convert a distance and angle between the wave gauge array and the reflection line to the properties of the reflected waves. *Genwaves2* and *Genwaves3D* are the functions that generates the wave elevation time series. *Applynoice* and *Savetowavelab* should be fairly self-explanatory.

After this the three methods returns all relevant properties to the main file, which plots the figures and and saves the generation and analyzed properties to a file.

D.3 Wave analysis

In the wave analysis three implemented methods are used, The piecewise constant method called *analysis_simple2*, the Maximum likelihood method called *analysis_MLM* and the modification of the MLM called *analysis_MMLM*. The three wave analysis are not comprised of as many distinguishable functions as the case is with wave generation. For this reason all three methods rely on just two notice-worthy functions, *crossspec* which calculates the auto- and cross spectral density functions and *wtok*¹ which calculates the wave numbers using the provided circular frequency. The rest of the procedure is handled internal in the three methods. The three analysis methods then returns the relevant estimated properties to the main function just as the case where for wave generation.

¹The script-name is meant as a acknowledgement of WAFO's w2k method, which was used in the early stages of the project.

This annex contains notes on various independent subjects.

E.1 The spectral density function

The auto- and cross-spectral density functions, referred to simply as the auto-spectra and cross-spectra, are denoted, $\Phi_{xx}(f)$ and $\Phi_{xy}(f)$ respectfully. They are defined in the frequency domain and are a central part of the stochastic analysis of ocean waves. The spectral density functions can be obtained in several ways. The two most common methods are through correlation functions and alternately through finite Fourier transforms. With known correlation functions it is possible to obtain the spectral density function by Fourier transforming the correlation function. This is done using the Wiener-Khinchine theorem shown in appendix E.3.2.

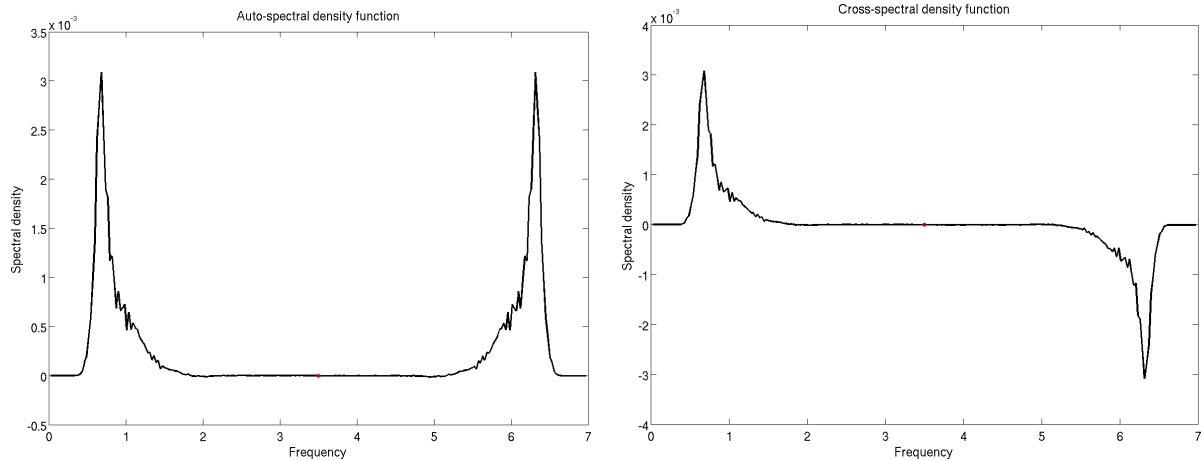
In this project the correlation functions are not known before hand, so instead the sample functions are Fourier transformed, this is the finite Fourier transform, the procedure of which is explained in detail in appendix A.

The auto-spectra is calculated to obtain fundamental properties of a single random process at different times. Similarly the cross-spectra is used to obtain the properties between two random processes. Essentially a spectral matrix may be created showing a visual interpretation of the relation between the auto- and cross-spectra, the matrix is shown in equation (E.1).

$$\begin{bmatrix} \Phi_{11} & \Phi_{21} & \dots & \Phi_{x1} \\ \Phi_{12} & \Phi_{22} & \dots & \Phi_{x2} \\ \vdots & \vdots & \ddots & \vdots \\ \Phi_{1y} & \Phi_{2y} & \dots & \Phi_{x=y} \end{bmatrix}$$

Where the diagonal are the auto-spectra and the off-diagonal are the cross-spectra. The properties of the two spectra are significantly different though, the auto-spectra are real-valued and even functions, unlike the cross-spectra which are complex functions. These properties are shown in equation (E.1) and illustrated in table E.1.

$$\begin{aligned} \Phi_{xx}(-f) &= \Phi_{xx}^*(f) = \Phi_{xx}(f) \\ \Phi_{xy}(-f) &= \Phi_{xy}^*(f) = \Phi_{yx}(f) \end{aligned} \tag{E.1}$$

Table E.1: Auto- and cross-spectral density function Φ_{xx} and Φ_{xy} .

E.2 Reflection

Reflection is quite a complicated matter. This section will only highlight some of the important aspects which should be considered when working with analytical methods on wave data with reflected waves. For further information on the subject see Davidson et al. (1998), Helm-Petersen (1998) and Isobe and Kondo (1984).

E.2.1 The reflection coefficient

The interpretation used in this project of reflection is that it is directly related to the wave amplitudes. Having a simple regular incident wave equation (E.2), the corresponding reflected wave is calculated by equation (E.3), where r is the so called reflection coefficient.

$$\eta_I = a \cdot \cos(\omega t) \quad (\text{E.2})$$

$$\eta_R = r \cdot a \cdot \cos(\omega t) \quad (\text{E.3})$$

As different regular waves are super-positioned into irregular waves and wave numbers are introduced, this reflection coefficient becomes a bit trickier to determine, as the reflection coefficient generally depends on the frequencies of the waves. This is important to remember when using methods which is supposed to determine these properties.

The determination of the reflection coefficient is entirely beyond the scope of this project, for further information on the subject it is suggested to read Helm-Petersen (1998) and Muttray et al. (2006).

E.2.2 The reflection line

The reflection line is the line at which the incident waves are reflected. As incident waves in this report is considered to span a azimuth range it also means that not all waves impact

on the reflection line at a 90 degree angle. This is where Snell's law is used to determine the direction of the reflected wave, for more on this see appendix E.4.

To further complicate the matter, not only the direction affects the reflected waves but also the slope of the reflector. Since the reflection coefficient varies with the frequencies the reflection line may lie in different places depending on which frequency the incident wave has.

E.3 Algorithms, theorems and methods implemented

This section covers the explanation of the algorithms, theorems and methods used throughout the project,

E.3.1 Euler's formula

References to Euler's formula in this project regards the formula used in complex analysis shown in equation (E.4).

$$e^{i\theta} = \cos(\theta) + i \cdot \sin(\theta) \quad (\text{E.4})$$

This equivalently means that the real and imaginary parts may be written as shown in equation (E.5).

$$\begin{aligned} \cos(\theta) &= \Re(e^{i\theta}) \\ \sin(\theta) &= \Im(e^{i\theta}) \end{aligned} \quad (\text{E.5})$$

Using the expression for waves in two and three dimensions,

$$\begin{aligned} \eta(x, t) &= a \cdot \cos(\omega t + kx + \Psi) \\ \eta(x, y, t) &= a \cdot \cos(\omega t + k(x \cdot \cos(\theta) + y \cdot \sin(\theta)) + \Psi) \end{aligned}$$

the corresponding exponential functions are shown in equation (E.6) and (E.7) respectfully.

$$\eta(\mathbf{x}, t) = a \cdot \Re\left(e^{i(\omega t + k\mathbf{x} + \Psi)}\right) \quad (\text{E.6})$$

$$\eta(x, y, t) = a \cdot \Re\left(e^{i(\omega t + k(x\cos(\theta) + y\sin(\theta)) + \Psi)}\right) \quad (\text{E.7})$$

E.3.2 Wiener-Khinchine Theorem

The Wiener-Khinchine theorem is a fundamental part of the signal processing used in this project, proving this theorem is beyond the scope however, see Bendat and Piersol (2000) instead. It relates the correlation from the time domain to the spectral density function from

the frequency domain.

$$S_{xx}(f) = \int_{-\infty}^{\infty} R_{xx}(\tau) e^{-i2\pi f\tau} d\tau \quad (\text{E.8})$$

$$S_{xy}(f) = \int_{-\infty}^{\infty} R_{yx}(\tau) e^{-i2\pi f\tau} d\tau \quad (\text{E.9})$$

$$R_{xx}(\tau) = \int_{-\infty}^{\infty} S_{xx}(f) e^{i2\pi f\tau} df \quad (\text{E.10})$$

$$R_{xy}(\tau) = \int_{-\infty}^{\infty} S_{yx}(f) e^{i2\pi f\tau} df \quad (\text{E.11})$$

Where S_{xx} and S_{xy} are the auto- and cross-spectral density functions and R_{xx} and R_{xy} are the auto- and cross-correlation functions.

E.3.3 Chebyshev's convergence optimization

Chebyshev suggested an optimization of the Newton-Raphson convergence theorem. It is used to obtain the wave-numbers through the dispersion relationship. This is done by expanding the Newton-Raphson solution seen in equation (E.12), with an additional term equation (E.13). While Chebyshev's method is slower for each iteration, the convergence should happen quicker resulting in an shorter execution time overall. Determining if this claim is true is outside the scope of this project. A more throughout explanation is found in Bagatur (2007).

$$\text{Newton-Raphson: } x_{i+1} = x_i - \frac{f(x_i)}{f'(x_i)} \quad (\text{E.12})$$

$$\text{Chebyshev: } x_{i+1} = x_i - \frac{f(x_i)}{f'(x_i)} - \frac{f^2(x_i)f''(x_i)}{f'^3(x_i)} \quad (\text{E.13})$$

Where $f''(x_i)$ denotes the second derivative while $f^2(x_i)$ is the function squared, and i indicates the iteration number.

E.3.4 Wave frequency to Wavenumber

The first usage of the Chebyshev Approximation is on the dispersion relationship and its derivatives seen in equation (E.14).

$$\begin{aligned} f(k) &= gk \tanh(kh) - \omega^2 \\ f'(k) &= g \tanh(kh) + gk \left(1 - \tanh(kh)^2\right) h \\ f''(k) &= 2g \left(1 - \tanh(kh)^2\right) h - 2gk \tanh(kh) \left(1 - \tanh(kh)^2\right) h^2 \end{aligned} \quad (\text{E.14})$$

The Matlab function implementing Chebyshev's optimization is named *wtok*, in the project.

E.3.5 Wave period to Wavelength

Similarly the Chebyshev Approximation is used on the expression yielded by Laplace's equation

$$\begin{aligned}
 f(L) &= \frac{1}{2} \frac{gT^2 \tanh\left(2 \frac{\pi h}{L}\right)}{\pi} - L & (E.15) \\
 f'(L) &= f - \frac{gT^2 \left(1 - \tanh\left(2 \frac{\pi h}{L}\right)^2\right) h}{L^2} - 1 \\
 f''(L) &= -\frac{4gT^2 \tanh\left(2 \frac{\pi h}{L}\right) \left(1 - \tanh\left(2 \frac{\pi h}{L}\right)^2\right) \pi h^2}{L^4} + \frac{2gT^2 \left(1 - \tanh\left(2 \frac{\pi h}{L}\right)^2\right) h}{L^3}
 \end{aligned}$$

The Matlab function implementing Chebyshev's optimization is named *TtoL*, in the project. Using $l_G < L/2$ defined by equation (5.1). Where l_G is the gauge distance and L is the wavelength. The relation between the gauge distance and the wave period is shown in figure E.1, using $h = 0.6$ in the range $T = 0.1$ to 1 .

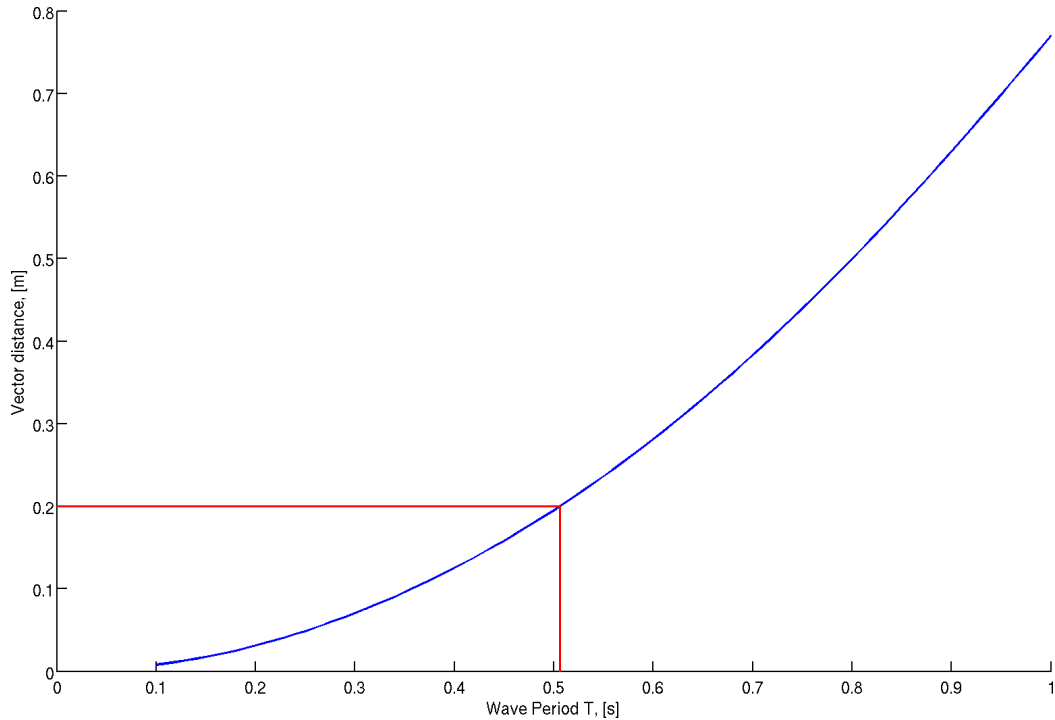


Figure E.1: Relation between gauge distance and wave period.

This means that for the minimum gauge separation (vector distance) of 0.2m can calculate wave periods no lower than $T \simeq 0.51$.

E.4 Geometry

This appendix explains the basic geometry used to define the reflection line, how the intersection between the incident wave direction and the reflection line are obtained and how this

can be used to calculate the direction of the reflected waves. This is used in connection with generation and analysis of bimodal waves, where the phase between incident and reflected waves are considered.

To keep the notation simple all “lines” are defined by and offset from the abscissa for simplicity and an angular direction in the plane. The abscissa and ordinate are hence forth referred to as x and y to keep notation simple.

coordinates in the plane are defined by equation (E.16).

$$\begin{aligned}x &= \cos(\theta) \cdot v + b \\y &= \sin(\theta) \cdot v\end{aligned}\tag{E.16}$$

Where θ is the angle of the line, v is an amplitude and b is the offset from the x-axis. This may be rewritten to an expression of y , see equation (E.17).

$$\begin{aligned}v &= \frac{y}{\sin(\theta)} = \frac{x - b}{\cos(\theta)} \\y &= (x - b) \cdot a, \text{ with } a = \frac{\sin(\theta)}{\cos(\theta)}\end{aligned}\tag{E.17}$$

Intersection between the two lines, $y = (x - b_1) \cdot a_1$ and $y = (x - b_2) \cdot a_2$, is then straight forward, and the x-coordinate of the intersection may be obtained by equation (E.18).

$$\begin{aligned}(x - b_1) \cdot a_1 &= (x - b_2) \cdot a_2 \\x &= \frac{a_2(x - b_2)}{a_1} + b_1\end{aligned}\tag{E.18}$$

Similarly the offset may obviously be calculated by equation (E.19).

$$b = x - \frac{y}{a}\tag{E.19}$$

Using Snell’s law in equation (E.20),

$$\frac{\sin(\theta_1)}{\sin(\theta_2)} = \frac{v_1}{v_2}\tag{E.20}$$

and assuming that the velocity change may be neglected the reflected wave direction may be calculated by mirroring it around the normal of the reflection line, and using equation (E.19) the corresponding offset may be obtained.

Bibliography

- Andersen, T. L., 2010. WaveLab. Version 3.0 and 3.34. Download: 03-05-2010.
URL <http://hydrosoft.civil.aau.dk/wavelab/index.htm>
- Andersen, T. L., Frigaard, P., 2008. Lecture notes for the course in, water wave mechanics. No. ISSN: 1901-7286. Aalborg University, dep. of Civil Engineering, Sohngaardsholmsvej 57, 9000 Aalborg.
- Andersen, T. L., Herdalur, P. M., Rzepka, S., 2002. Wblcalc -wave boundary layer calculation. Download: 18-05-2010.
URL <http://people.civil.aau.dk/~i5t1a/B8K/kysthydr/WBLCalcsetupNT-2000-XP.exe>
- Ayyub, B. M., McCuen, R. H., 06 2002. Probability, Statistics and Reliability for engineers and scientists, 2nd Edition. Taylor & Francis Inc.
- Bagatur, T., 2007. Modified newton-raphson solution for dispersion equation of transition water waves. Journal of Coastal Research 23 (6), 1588–1592.
- Barber, N., Doyle, D., 1956. A method of recording the direction of travel of ocean swell. In: Deep Sea Research. Vol. 3. pp. 206–210.
- Barber, N. F., 1963. The directional resolving power of an array of wave detectors. In: Ocean Wave Spectra. Prentice-Hall, inc., pp. 137–150.
- Bendat, J. S., Piersol, A. G., 2000. Random Data: Analysis and Measurement Procedures, 3rd Edition. Wiley Series in Probability and Statistics. John Wiley & Sons, Inc., Danvers, MA.
- Benoit, M., Frigaard, P., Schäffer, H., Aug. 1997. Analysing multidirectional wave spectra: A tentative classification of available methods. In: IAHR Seminar Multidirectional Waves and their Interaction with Structures. 27th IAHR Congress. The International Association for Hydro-Environment Engineering and Research, The National Research Council of Canada.
- Benoit, M., Teisson, C., 1994. Laboratory comparison of directional wave measurement systems and analysis techniques. In: IAHR Seminar Multidirectional Waves and their Interaction with Structures. 27th IAHR Congress. The International Association for Hydro-Environment Engineering and Research, The National Research Council of Canada.
- Borgman, L. E., Panicker, N. . N., 1970. Design study for a suggested wave gage array off point mogu, california. Tech. Rep. 1-14, Hydraulic Engrg. Lab., Univ. Calif., Berkeley, California.
- Brüel, Kjær, sep 1987. Frequency analysis, 3rd Edition. K. Larsen & Søn A/S, Glostrup, Denmark.
- Capon, J., Greenfield, R. J., Kolker, R. J., feb 1967. Multidimensional maximum-likelihood processing of a large aperture seismic array. In: Proceedings of the IEEE. Vol. 55. IEEE, pp. 192–211.
- D., P. W., may 1999. Natural Sciences Citations and References (natbib). 7th Edition.
- Davidson, M. A., Huntley, D. A., Bird, P. A., may 1998. A practical method for the estimation of directional wave spectra in reflective wave fields 33 (2-3), 92–116.
- Davis, R. E., Regier, L. A., aug 1977. Methods for estimating directional wave spectra from multi-element arrays. Journal of marine research 35 (3), 453–477.
- Fernandes, A. A., Gouveia, A. D., Nagarajan, R., 1988. Determination of wave direction from linear and polygonal arrays. Ocean Engineering 15 (4), 345–357.

- Frigaard, P., Helm-Petersen, J., Klopman, G., Stansberg, C., Benoit, M., Briggs, M., Miles, M., Santas, J., Schäffer, H., Hawkes, P., 1997. Iahr list of sea state parameters - an update for multidirectional waves. In: IAHR Seminar Multidirectional Waves and their Interaction with Structures. 27th IAHR Congress. The International Association for Hydro-Environment Engineering and Research, The National Research Council of Canada.
- Goda, Y., 1988. Statistical variability of sea state parameters as a function of wave spectrum. Coastal Engineering Journal 31 (2), 39–52.
- Goda, Y., mar 1999. A comparative review on the functional forms of directional wave spectrum. Coastal Engineering Journal 41 (1), 1–20.
- Goda, Y., aug 2008. Overview on the applications of random wave concept in coastal engineering. Proceedings of the Japan Academy. Series B, Physical and biological sciences 84 (9), 374–385.
- Goda, Y., 2010. Random seas and design of maritime structures, 3rd Edition. Vol. 33 of Advanced Series on Ocean Engineering. World Scientific Publishing Co. Pte. Ltd., 5 Tok Tuck Link, Singapore.
- Hasselmann, K., Barnett, T., Bouws, E., Carlson, H., Cartwright, D., Enke, K., Ewing, J., Gienapp, H., Hasselmann, D., Kruseman, P., Meerburg, A., Müller, P., Olbers, D., Richter, K., Sell, W., Walden, H., 1973. Measurements of wind-wave growth and swell decay during the joint north sea wave project (jonswap). Ergänzungsheft zur Deutschen Hydrographischen Zeitschrift Reihe A(8) (12), 95.
- Haubrich, R. A., 1968. Array design. Bulletin of the Seismological Society of America 58 (3), 977–991.
- Hawkes, P., 1997. Iahr database, case 6: Multidirectional wave data analysis. Website, download: 24-05-2011.
URL http://www.iahr.net/site/e_library/links/databases/default.html
- Hawkes, P., Ewing, J., Harford, C., Klopman, G., Stansberg, C., Benoit, M., Briggs, M., Frigaard, P., Hiraishi, T., Miles, M., Santas, J., Schäffer, H., aug 1997. Comparative analyses of multidirectional wave basin data. In: IAHR Seminar Multidirectional Waves and their Interaction with Structures. 27th IAHR Congress. The International Association for Hydro-Environment Engineering and Research, The National Research Council of Canada.
- Helm-Petersen, J., oct 1998. Estimation of wave disturbance in harbours. Master's thesis, Aalborg University.
- Heteren, J., 1983. Estimation of multi-modal directional wave spectra from tri-orthogonal measurements. Coastal Engineering 7 (3), 205–231.
- Hughes, S. A., Dec. 1984. The tma shallow-water spectrum description and applications. Tech. Rep. ADA157975, COASTAL ENGINEERING RESEARCH CENTER, VICKSBURG MS.
URL <http://oai.dtic.mil/oai/oai?verb=getRecord&metadataPrefix=html&identifier=ADA157975>
- Isobe, M., Kondo, K., 1984. Method for estimating directional wave spectrum in incident and reflected wave field. In: Edge, B. L. (Ed.), Coastal Engineering 1984 Proceedings. Vol. 1. American Society of Civil Engineers, American Society of Civil Engineers, ASCE, pp. 467–483.
- Isobe, M., Kondo, K., Horikawa, K., Jun. 1984. Extension of mlm for estimating directional wave spectrum. In: Symposium on Description and Modelling of Directional Seas., Vol. A6. DHI & MMI, pp. 1–15.
- Kofoed, J. P., 2009. PH. D. course in Experimental Testing for Wave Energy Utilization: Introduction - Wave reflection. Aalborg University, lecture 7: Reflection analysis of waves. Download: 03-05-2010.
URL http://www.waveenergy.civil.aau.dk/we_phd_course/2009/we_phd_course.htm
- Liu, Z., Frigaard, P., 2001. Generation and analysis of random waves. No. ISBN: Unknown. Department of Civil Engineering at Aalborg University.
- Longuet-Higgins, M., Cartwright, D., Smith, N., 1963. Observation of the directional spectrum of sea waves using the motions of a floating buoy. In: Conference on Ocean Wave Spectra. pp. 111–132.

- Marple, S. L., mar 1987. Digital spectral analysis, with applications, 1st Edition. Vol. 1 of Prentice hall signal processing series. Prentice-Hall, inc., Englewood Cliffs. NJ, USA.
- MetOcean Solutions LTD, 2002. DIWASP, a directional wave spectra toolbox for MATLAB. Centre for Water Research, University of Western Australia, Perth.
URL <http://www.metocean.co.nz/cms/>
- Mitsuyasu, H., Tasai, F., Suhara, T., Mizuno, S., Ohkusu, M., Honda, T., Rikiishi, K., 1975. Observations of the directional spectrum of ocean waves using a cloverleaf buoy. *Journal of physical oceanography* 5 (2), 750–760.
- Muttray, M., Oumeraci, H., Oever, E., 2006. WAVE REFLECTION AND WAVE RUN-UP AT RUBBLE MOUND BREAKWATERS. Engineering. San Diego, download: 18-05-2010.
URL <http://www.xbloc.com/downloads>
- Ochi, M. K., 1998. Ocean waves, the stochastic approach, 1st Edition. Vol. 6 of Cambridge ocean technology. Press syndicate of the university of Cambridge, The Pitt Building, Cambridge, UK.
- Pawka, S., 1974. Study of wave climate in nearshore waters. In: *Symposium on Ocean Wave Measurement and analysis*. Vol. 1. pp. 745–760.
- Pierson, W. J., Neumann, G., James, R. W., 1955. Practical methods for observing and forecasting ocean waves by means of wave spectra and statistics. H.O. pub. (603), 284.
- Sand, S. E., 1979. Three-dimensional deterministic structure of ocean waves. Ph.D. thesis, Technical University of Denmark, Lyngby, Denmark.
- Scott, C., Nowak, R., may 2004. Maximum likelihood estimation. Download: 28-02-2011.
URL <http://cnx.org/content/ml1446/latest/>
- The Mathworks, 2010. Using FFT to Obtain Simple Spectral Analysis Plots. Download: 03-05-2010.
URL <http://www.mathworks.com/support/tech-notes/1700/1702.html>
- Tsanis, I. K., Brisette, F. P., 1992. Wave directional spectra measurements by small arrays in lake ontario. *J. Great Lakes Res.* 18 (3), 489–506.
- U.S. Army Engineer, Jun. 1985a. Directional wave spectra using cosine-squared and cosine 2s spreading functions. Tech. Rep. CETN-I-28, COASTAL ENGINEERING RESEARCH CENTER, VICKSBURG MS.
- U.S. Army Engineer, Mar. 1985b. Directional wave spectra using normal spreading function. Tech. Rep. CETN-I-6, COASTAL ENGINEERING RESEARCH CENTER, VICKSBURG MS.
- U.S. Army Engineer, Sep. 1992. Importance of directional spreading of waves in the nearshore region. Tech. Rep. CETN-I-53, COASTAL ENGINEERING RESEARCH CENTER, VICKSBURG MS.
- U.S. Army Engineer, Oct. 1994. Spectral wave modelling technology. Tech. Rep. CETN-I-58, COASTAL ENGINEERING RESEARCH CENTER, VICKSBURG MS.
- WAFO-group, 2000. WAFO - A Matlab Toolbox for Analysis of Random Waves and Loads - A Tutorial. *Math. Stat.*, Center for Math. Sci., Lund Univ., Lund, Sweden.
URL <http://www.maths.lth.se/matstat/wafo>